

Distribution Agreement

In presenting this thesis or dissertation as a partial fulfillment of the requirements for an advanced degree from Emory University, I hereby grant to Emory University and its agents the non-exclusive license to archive, make accessible, and display my thesis or dissertation in whole or in part in all forms of media, now or hereafter known, including display on the world wide web. I understand that I may select some access restrictions as part of the online submission of this thesis or dissertation. I retain all ownership rights to the copyright of the thesis or dissertation. I also retain the right to use in future works (such as articles or books) all or part of this thesis or dissertation.

Signature:

Cassandra Buru

Date

Modular Synthesis of Asymmetric Triazacyclononane Derivatives and Potential Aerobic
Copper Oxidation Catalyst Supported by a Bridging Bulky Triazacyclononane

By

Cassandra Buru
Master of Science

Chemistry

Christopher Scarborough, Ph.D.
Advisor

Craig Hill, Ph.D.
Committee Member

Cora MacBeth, Ph.D.
Committee Member

Accepted:

Lisa A. Tedesco, Ph.D.
Dean of the James T. Laney School of Graduate Studies

Date

Modular Synthesis of Asymmetric Triazacyclononane Derivatives and Potential Aerobic
Copper Oxidation Catalyst Supported by a Bridging Bulky Triazacyclononane

By

Cassandra Buru

Advisor: Christopher Scarborough, Ph.D.

An abstract of
A thesis submitted to the Faculty of the
James T. Laney School of Graduate Studies of Emory University
in partial fulfillment of the requirements for the degree of
Master of Science
in Chemistry
2015

Abstract

Modular Synthesis of Asymmetric Triazacyclononane Derivatives and Potential Aerobic Copper Oxidation Catalyst Supported by a Bridging Bulky Triazacyclononane By Cassandra Buru

Metalloenzymes carry out synthetically challenging oxidations, usually involving an earth abundant bimetallic center and atmospheric oxygen. 1,4,7-triazacyclononane (tacn) derivatives have historically been used to model the active sites in these enzymes. However, above cryogenic temperatures, these model systems oxidize the ligand, preventing catalysis at ambient temperatures. Until recently, there had been no precedent for creating bulky substituents on tacn to prevent ligand degradation. This report will describe the scope of the ^tBu₃tacn synthesis to other tacn derivatives, in particular, to binucleating tacn derivatives with *tert*-butyl substituents, and the corresponding coordination chemistry. Furthermore, studies on intramolecular oxidation of these bimetallic complexes will be described. Finally, preliminary results will demonstrate progress to prevent ligand degradation.

Modular Synthesis of Asymmetric Triazacyclononane Derivatives and Potential Aerobic
Copper Oxidation Catalyst Supported by a Bridging Bulky Triazacyclononane

By

Cassandra Buru

Advisor: Christopher Scarborough, Ph.D.

A thesis submitted to the Faculty of the
James T. Laney School of Graduate Studies of Emory University
in partial fulfillment of the requirements for the degree of
Master of Science
in Chemistry
2015

Acknowledgements

My family and friends, especially Eric Erby

Research advisor: Christopher Scarborough, Ph.D.

Committee members: Cora Macbeth, Ph.D.; Craig Hill, Ph.D.

Group members: Gregory Karahalos, Christian Wallen, Thomas Pickel

Former group members, especially Jack Trieu; Aru Thangavel, Ph.D.

John Bacsa, Ph.D. and Marika Wieliczko for X-ray crystallographic assistance and structures

Frederick Strobel, Ph.D.; Elizabeth Magnotti of Mass Spectroscopy Center

Jose Soria and the survivors of his freshman organic for the inspiration to pursue research and for intellectual challenges/discussions

Jacob Shreckengost, Caitlin Davis, Emory Clare Boothe Luce Fellows, and CBL Foundation for professional development and support

Table of Contents

Section	Page
1.0 Introduction: An Oxidation Problem	1
1.1 Oxidations in Biology	
1.2 Copper and Dioxygen in Synthetic Systems	
1.2.1 Binucleating Systems	
1.2.2 Ligand Degradation	
1.3 Previous Derivatives of tacn	
1.4 Goals of the Project	
2.0 Results and Discussion	11
2.1 Alternative Synthesis to Known tacn Derivatives	
2.2 Di- and Mono- <i>tert</i> -butyl tacn	
2.3 Bridging tacn Synthesis	
2.4 Bridging Copper tacn Complexes	
3.0 Future Studies	22
3.1 Spectroscopic Studies	
3.2 New Bridging Ligands	
3.2.1 Aryl-Bridging Unit	
3.2.2 Methyl-Protected Bridging Unit	
4.0 Conclusions	25
5.0 Experimental	26
5.1 General Considerations	
5.2 Ligand Syntheses	
5.2.1 Chloro-acetylation	
5.2.2 Cyclizations	
5.2.3 Oxidation/Reductions	
5.3 Metal Complexes	
6.0 Supporting Information	34
7.0 References	44
List of Charts	Page
1. Possible Binding Modes of Copper/Oxygen Centers	2
2. Karlin's (left) and Tolman's (right) Binucleating Scaffolds	6
3. Degradations of tacn Derivatives	7
4. <i>Top</i> : Crystal Structure of Cu(I)- ^t Bu ₂ dtne (MeCN) ₂ (PF ₆) ₂ <i>Bottom</i> : Crystal Structure of Cu(I)- ^t Bu ₂ dtnp (MeCN) ₂ (PF ₆) ₂ (hydrogens and counter-anions omitted for clarity)	18
5. Cu- ^t Bu ₂ dtne (MeCN) ₂ (PF ₆) ₂ at -40°C 3-6 hours after exposure to O ₂	20
6. Overlay UV-vis spectra of Cu- ^t Bu ₂ dtne (OTf) ₂ in red and Cu- ^t Bu ₂ dtnp (OTf) ₂ in purple in DCM 5 minutes after exposed to air	21
7. ¹ H NMR of <i>N,N'</i> -Bis(2-chloroacetyl)- <i>N,N'</i> -dimethyl-ethylene-diamine (6). Sets of peaks identified as amide rotamers. (* impurities, Δ solvent)	34
8. Rotamer region ¹ H NMR of <i>N,N'</i> -Bis(2-chloroacetyl)- <i>N,N'</i> -dimethyl-ethylene-diamine (6)	34

List of Charts Continued	Page
9. Mass spec of polymerized product of <i>N,N'</i> -Bis(2-chloroacetyl)- <i>N,N'</i> -dimethyl-ethylene-diamine with benzyl amine	35
10. Preliminary mass spec result for 2,3-bis(4,7-di- <i>tert</i> -butyl-1,4,7-triazonan-1-yl-2,6-dione)-2,3-dimethyl-propane	35
11. UV-vis of Cu(I)- ^t Bu ₂ dtne(MeCN) ₂ PF ₆ before exposure to O ₂	36
12. UV-vis of Cu- ^t Bu ₂ dtne final product after exposure to O ₂	36

List of Figures	Page
1. Cobalt complex of Bn ^t Bu ₃ tacn (hydrogens and counter-anions omitted for clarity)	14
2. Crystal structure of the linear product formed with trityl amine (hydrogens omitted for clarity)	14
3. Crystal Structure of H ^t Bu ₂ tacn (hydrogens omitted for clarity)	15
4. Crystal structure of 1,2-bis(4,7-di- <i>tert</i> -butyl-1,4,7-triazonan-1-yl)ethane (hydrogens omitted for clarity)	16
5. Crystal Structure and ChemDraw of Cu- ^t Bu ₂ dtne (MeCN) ₂ (PF ₆) ₂ after O ₂ exposure (hydrogens and counter-anions omitted for clarity)	19

List of Schemes	Page
1. Traditional Synthesis and Substitutions on tacn	8
2. Traditional Synthesis of Substituted Bis-tacn	9
3. Reported synthesis of ^t Bu ₃ tacn	9
4. Chloro-acetylation step	11
5. Attempted cyclization of 6	11
6. <i>Top</i> : Methyl substituted derivative favors equilibrium to the right. <i>Bottom</i> : <i>Tert</i> -butyl substituted derivative favor equilibrium to the left due to steric interactions	12
7. Synthesis of Bn ^t Bu ₃ tacn	13
8. Possible cyclizations with 4 and EDA	16
9. Target aryl-bridged ligand	23
10. Target methyl protected ethane bridge	24

List of Tables	Page
1. Approximate UV-vis Transitions for Selected Binding Modes	4
2. Crystal Data for Cobalt (I) 1,4-di- <i>tert</i> -butyl-7-benzyl-1,4,7-triazacyclononane	37
3. Crystal Data for <i>N,N'</i> -diaminotrityl-3,8-diacetyl-4,7-di- <i>tert</i> -butyl-ethylene-diamine (Figure 2)	38
4. Crystal Data for 1,4-di- <i>tert</i> -butyl-1,4,7-triazacyclononane	39
5. Crystal Data for 1,2-bis(4,7-di- <i>tert</i> -butyl-1,4,7-triazonan-1-yl)ethane	40
6. Crystal Data for Copper (I) 1,2-bis(4,7-di- <i>tert</i> -butyl-1,4,7-triazonan-1-yl)ethane (BF ₄) ₂	41
7. Crystal Data for Copper (I) 1,2-bis(4,7-di- <i>tert</i> -butyl-1,4,7-triazonan-1-yl)propane (BF ₄) ₂	42
8. Crystal Data for Oxidized Copper 1,2-bis(4,7-di- <i>tert</i> -butyl-1,4,7-triazonan-1-yl)ethane (BF ₄) ₂	43

Common Abbreviations

Bn	benzyl
DDQ	2,3-Dichloro-5,6-dicyano-1,4-benzoquinone
dtne	1,2-bis(4,7-di- <i>tert</i> -butyl-1,4,7-triazonan-1-yl)ethane
dtnp	1,2-bis(4,7-di- <i>tert</i> -butyl-1,4,7-triazonan-1-yl)propane
EDA	ethylene diamine
^{m_3}O	bis(μ_3 -oxo)
Me	methyl
^mO	bis(μ -oxo)
OAc	acetate
OTf	triflate
PMB	para-methoxy benzyl
pMMO	particulate methane mono-oxygenase
SO	η^1 -superoxo
^sP	side-on peroxo, μ - η^2 : η^2 -peroxo
tacn	1,4,7-triazacyclononane
^tBu	<i>tert</i> -butyl
tmpa	5 tris[(2-pyridyl)-methyl]amine
^TP	trans- μ -1,2-peroxo
XAFS	X-ray absorption fine structure

1.0 Introduction: An Oxidation Problem

Oxidation reactions play important roles in organic syntheses, biochemistry, and industrial processes. To obtain useful organic chemicals industrially, petrochemical feedstock must undergo controlled partial oxidation of simple hydrocarbons¹, such as the conversion of benzene to phenol. Current industrial standards for these transformations require high temperatures and pressures, creating hazardous working conditions and high operating costs². Catalysts have been developed in laboratories to perform controlled oxidations under mild conditions; however, a majority of these catalysts utilize second- or third-row transition metals: rhodium, palladium, ruthenium, and iridium³. These rare-earth metals cost much more than their first-row counterparts⁴. Furthermore, these syntheses employ a stoichiometric amount of inorganic oxidants, like chromate and permanganate⁵. The toxic inorganic by-products from these reactions prevent their use in industrial processes. An ideal process would employ a first-row transition metal, in conjunction with atmospheric oxygen to perform catalytic oxidation under mild conditions.

The problem with using 3d metals is the poor reactivity and selectivity which arises because of the relatively small size of the orbitals. As a result, these first-row transition metals prefer to perform one-electron processes, instead of the two-electron processes which dominate organic transformations³. Copper, like other late first-row transition metals, can access oxidation states I-III without changing ligand scaffolds. This property potentially makes copper suitable for use as a molecular catalyst in one- and two-electron processes⁶. Enzymes in Nature are capable of exploiting this property and utilizing first-row transition metals for organic transformations with high selectivity⁷.

1.1 Oxidations in Biology

Metalloenzymes in cells affect important chemical transformations, often involving small molecule activation⁷. The most prevalent metal centers in these enzymes use iron, manganese, and/or copper in the active site. Copper proteins that bind and/or activate dioxygen perform critical biological functions. Among these functions are O₂ transportation (hemocyanin), aromatic ring oxidation (tyrosinase, catechol oxidase, and laccase), and methane oxidation (particulate methane monooxygenase [pMMO])⁸.

Oxygen can adopt different binding modes, depending on the ratio of copper to oxygen. The most prevalent binding modes are shown in **Chart 1**.

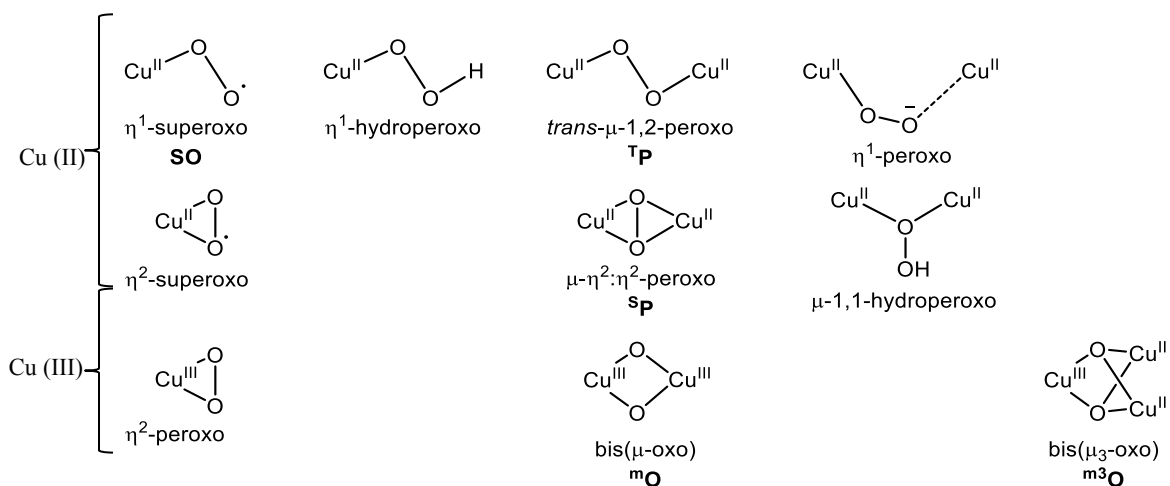


Chart 1. Possible Binding Modes of Copper/Oxygen Centers¹⁶

Important to note is that these structures exist in equilibrium, so that multiple modes can exist simultaneously^{8,9,10}. The structures of each mode determine the types of reactivity they undergo. For example, **^sP** species affect aromatic hydroxylations, and **^mO** species are capable of H-atom abstraction¹¹.

Copper proteins can be classified according to the structure of their active site. For example, type 3 copper centers consist of a pair of copper centers, each coordinated by three histidine residues. Type 3 copper proteins (tyrosinase, hemocyanin and catechol oxidases) appear to reversibly bind O₂ by two Cu (I) ions in a $\mu\text{-}\eta^2\text{-}\eta^2$ peroxo mode^{11,12}. This dinuclear ^sP is the only confirmed Cu/O₂ active species in biology¹¹. Though studies have confirmed the di-copper active site in pMMO¹³, further work needs to determine which Cu/O₂ mode the core adopts. The reactivity differences of type 3 copper proteins, despite similar active sites, have intrigued researchers for a long time¹⁴. These aerobic copper reactions are particularly prevalent in biological systems, and the mechanisms by which these enzymes catalyze reactions have been extensively studied, yet some remain elusive¹⁵. Many attempts have been made to synthetically replicate these active sites¹⁶.

1.2 Copper and Dioxygen in Synthetic Systems

Synthetic systems seek to mimic the reactivity found in nature. The development of these synthetic systems is two-fold. First, these models aim to better understand the catalytic processes in biomolecules. Second, they assist the development of new catalysts under mild conditions^{1,17}. These systems are not new to the literature and have been extensively studied.

Cu/O₂ adducts have been shown to perform oxidative transformations on alkyl, allylic, and benzylic positions⁶. Additionally, copper can catalyze oxidative arene coupling and Baeyer-Villager type reactions⁶. These reactions employ a heterogeneous catalyst like CuCl₂ or Cu(OAc)₂, which are plagued with unwanted side reactions and oligomerizations⁶. In homogenous catalysis, ligands can be constructed to mimic an

active site and support transitive oxidations states¹⁶. The intermediates can therefore be stabilized and the active species determined spectroscopically¹⁷. For example, each binding mode in **Chart 1** has unique charge transfer absorptions dependent on the different splitting of the d orbitals by the dioxygen (ligand field theory)¹⁶. **Table 1** shows the most prevalent binding modes in the literature along with the characteristic UV-vis absorptions.

Table 1. Approximate UV-vis Transitions for Selected Binding Modes

<i>species</i>	<i>UV-vis: λ, nm (ϵ, $mM^{-1}cm^{-1}$)</i>	<i>reference</i>
^TP	530 (10), 600 (sh, 7)	10,16
^SP	360 (24), 520 (1)	16
^mO	300 (20), 400 (24)	16
^{m3}O	340 (12), 500 (1), 680 (0.8)	18, 19
SO	400 (4), 570 (0.8), 700 (1)	20,21

As noted before, these binding modes also exist in equilibrium; this property can be reflected in the UV-vis as a combination of two or more sets of features^{10,15}. The binding mode and UV-vis signatures are strongly dependent on the steric environment, chelation, and donor strength surrounding the copper center^{15,16,22,23,24}.

The distinction between these binding modes by UV-vis features is not always clear. Itoh's proposed tri-nuclear copper has features at 340, 500, and 680 nm. Earlier reports propose the active oxygen intermediate is a hydro-peroxo with features at 340, 470, and 680 nm²⁵. Another report proposed a peroxo intermediate with features at 340, 475, and 680 nm²⁶. The features among the three spectra are similar in size, shape and energy, so another method must be utilized to determine the observed active species.

Resonance Raman and XAFS can better differentiate between the binding modes by the unique ro-vibrational transitions²⁷. X-ray crystallography is the most descriptive technique for structural characterization; however, these Cu/O₂ complexes are thermally sensitive^{6,8,16,27}, rendering crystallization of most complexes difficult. Examples of Cu/O₂ adducts stable at room-temperature are rare⁸, so UV-vis, resonance Raman, and XAFS remain the primary methods for structure determination even after the development of X-ray crystallography²⁷.

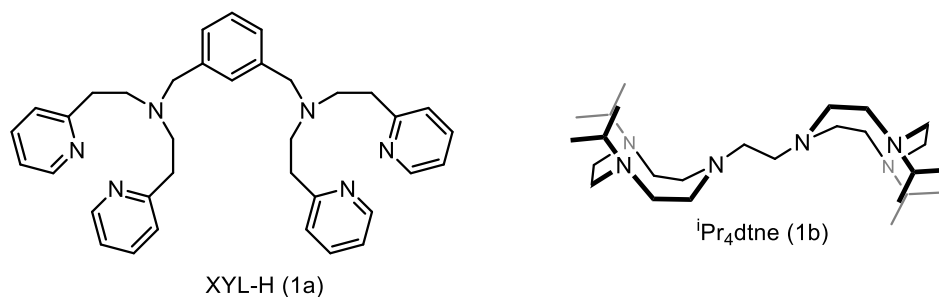
Definitive structural characterization of copper-oxygen complexes was first made possible by Karlin and coworkers in 1988¹. In the report, a crystal of a copper trans- μ -1,2 peroxo supported by tmpa (5 tris[(2-pyridyl)-methyl]amine) was synthesized and characterized at -80°C²⁸. Soon after, Kitajima and coworkers reported the first copper μ - η^2 - η^2 peroxo crystal, supported by tris-pyrazol borate (hydrido-tris(3,5-isopropyl)pyrazolylborate)²⁹. Since then, lengthy reviews have summarized the model systems^{6,8,16,27}.

1.2.1 Bi-Nucleating Synthetic Systems

Among the literature examples, bridging bi-nucleating ligand scaffolds with three nitrogen donors have found particular relevance. Not only because Nature uses a two-copper motif, but also because mononuclear copper complexes will often dimerize spontaneously in the presence of O₂^{8,16}. A bridging scaffold encourages this cooperation between the copper centers to enforce a di-nuclear site, which tyrosinase, catechol oxidase, and hemocyanin utilize.

Two extensively studied binucleating systems are from Karlin and Tolman. Karlin's **1a** utilizes tmpa (tris(2-pyridylmethyl)amine) donors with a bridging xylene linker²⁸ (**Chart 2**) while Tolman's **1b** employs tacn (1,4,7 triazacyclononane) donors with alkyl (**Chart 2**) and xylene linkers¹⁵ (**Chart 3**).

Chart 2. Karlin's (left) and Tolman's (right) Binucleating Scaffolds



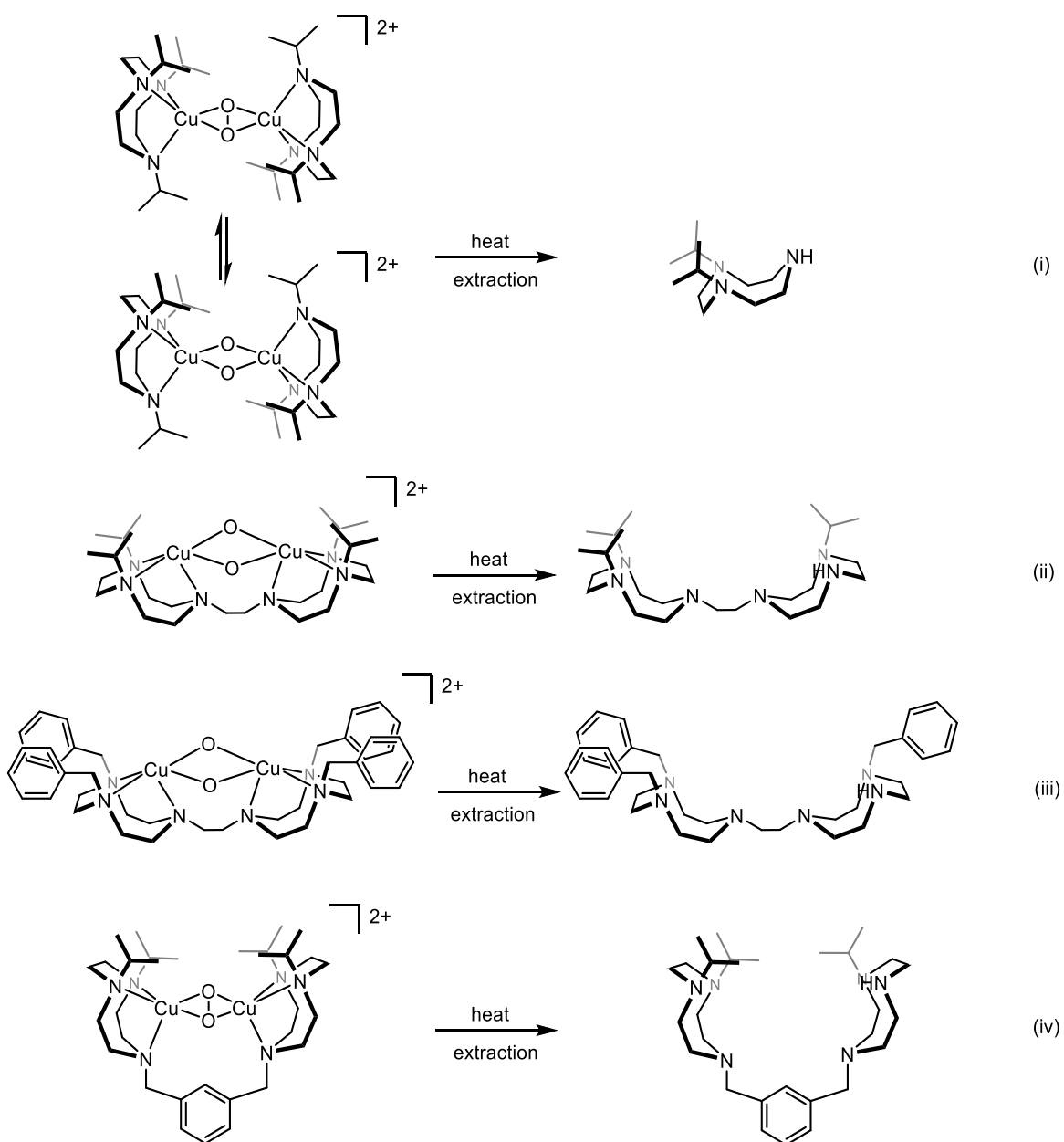
Upon complexation with a Cu(I) source, both ligands support two copper sites that are poised in close proximity. When exposed to atmospheric oxygen at low temperature, the **1a** copper(I) complex forms a ^s**P**³⁰. Alternatively, the **1b** copper(I) complex binds dioxygen at low temperature in a ^m**O** mode exclusively³¹. The mono-nuclear form of **1b**, ⁱPr₃tacn, yields a mixture of the ^s**P** and ^m**O** modes. When the **1b** ethylene bridge is substituted with a xylene, similar to **1a**, the ^s**P** is formed³¹. Since the development of these two ligands, other derivatives have been synthesized and studied by various groups^{6,16}.

1.2.2 Ligand Degradation

Some reactivity of Cu/O₂ complexes with substrates has been explored at low temperature⁹. However, above -70°C, the O₂ core reacts with the closest CH bond on the ligand, and prevents further oxidations¹⁷. For example Karlin's ligand, upon degradation,

performs aromatic hydroxylation of the xylene on the bridge³². Tolman's ligands undergo aliphatic hydroxylation of the carbon α to the amine of tacn³³. Even when a xylene bridge is incorporated into the scaffold, the degradation occurs on the α -amino CH bond³⁴. The degradation pathways of bridging tacn are summarized in **Chart 3**.

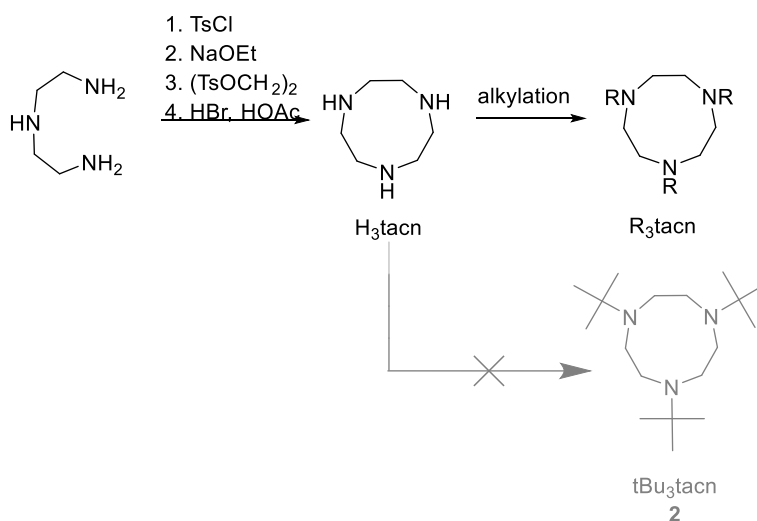
Chart 3. Degradations of tacn Derivatives



To study the reactivity of tacn species at ambient conditions and prevent ligand degradation, the α -amino CH bonds on the nitrogen substituents must not exist³⁵. Until recently, there had been no literature precedence for creating these bulky alkyl substituents on tacn⁴⁶.

1.3 Previous Derivatives of tacn

Simplest derivative of 1,4,7-triazacyclononane (tacn) is the tridentate macrocycle H₃tacn. This ligand scaffold is electronically flexible, so tacn is able to stabilize low- and high-valent transition metals. Prior to 2013, the only route to tacn and its derivatives is shown in **Scheme 1**³⁶.

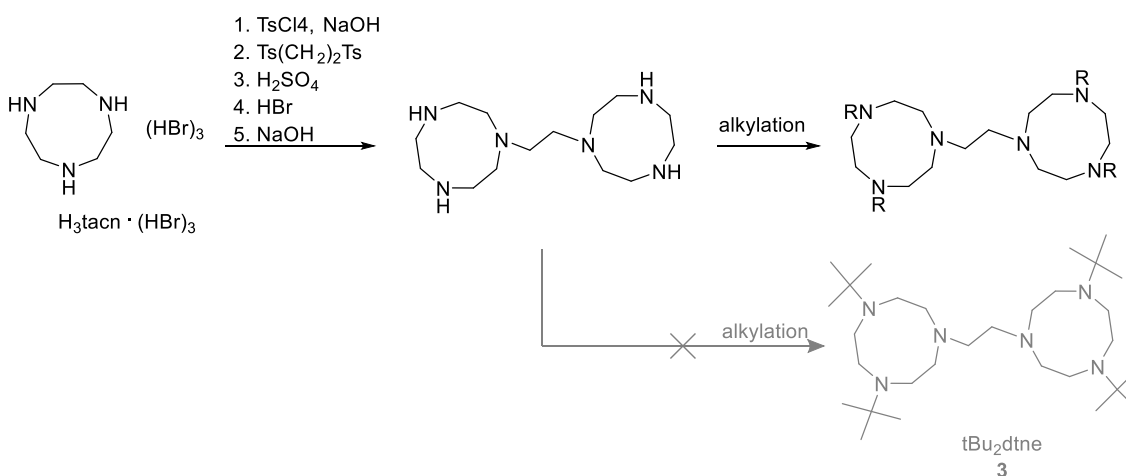


Scheme 1. Traditional Synthesis and Substitutions on tacn

After de-tosylation, H₃ tacn can be transformed into a number of possible derivatives via an S_N2 reaction between nitrogens and an alkyl halide. This transformation is not possible with tertiary alkyl halides due to the steric hindrance and poor orbital overlap. Ligand **2**

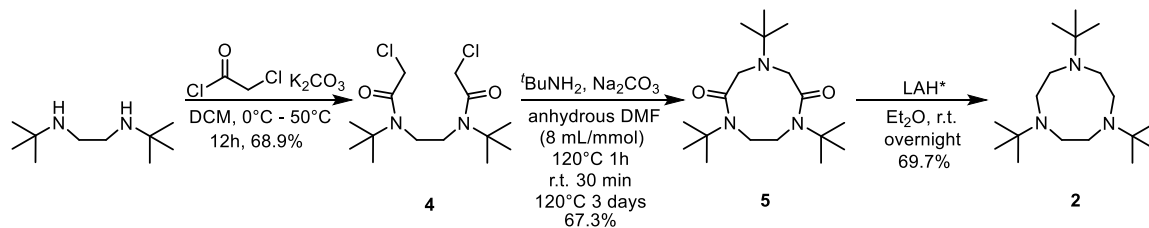
(1,4,7-tri-*tert*-butyl-1,4,7-triazacyclononane) cannot be synthesized via this traditional route.

Similarly, bis-tacn moieties could be obtained from H_3tacn ³⁷, **Scheme 2**. The simplest bridging NH-tacn could be obtained in 38% yield in 5 steps by this method. However, installing tertiary alkyl substituents on the remaining nitrogens was again impossible via traditional alkylation routes to ligand **3** (1,2-bis(1,4-di-*tert*-butyl-1,4,7-triazonane-1-yl)ethane).



Scheme 2. Traditional Synthesis of Substituted Bis-tacn

To circumvent this problem, the Scarborough lab needed to develop an alternate synthetic pathway using preinstalled tertiary alkyl substituents on the nitrogens. A paper published on aza-crown compounds provided the necessary link. In the report, two chloroacetyl groups were placed in close proximity that allowed ring closure. Reduction of the amide yielded their desired aza macrocycles³⁸. The procedure was applied to di-*tert*-butyl ethylene diamine to yield tBu_3tacn (1,4,7-tri-*tert*-butyl 1,4,7-triazacyclononane)⁴⁶ by **Scheme 3**.



Scheme 3. Reported synthesis of ^tBu₃tacn

In the first step of **Scheme 3**, a chloro-acetylation reaction places two acetyl groups in close proximity to yield **4**. Cyclization occurs with the addition of a primary amine in the second step to obtain **5**. Finally, LiAlH₄ reduces the amides for the desired ^tBu₃tacn. Future work would optimize the reaction conditions and modulate the synthesis for this ligand scaffold, increasing the yield and widening the scope of the methodology. Additionally, these ligands would be metallated and exposed to small molecules to determine reactivity.

1.4 Goals of Project

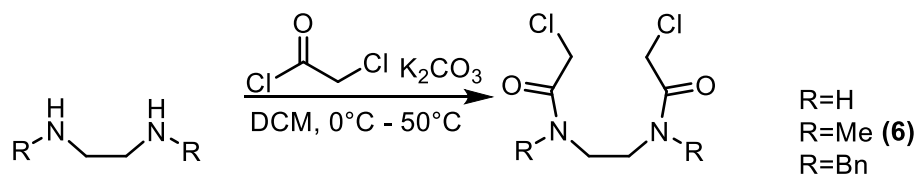
The goals of this project are:

1. Apply ^tBu₃tacn synthesis to shortcut route to other tacn species.
2. Synthesize H^tBu₂tacn by protection and subsequent deprotection of one amine functional group.
3. Apply the methodology developed in the previous goals to develop a bridging tacn synthesis.
4. Create a bi-nucleating copper catalyst based on tethered ^tBu₂tacn.

2.0 Results and Discussion

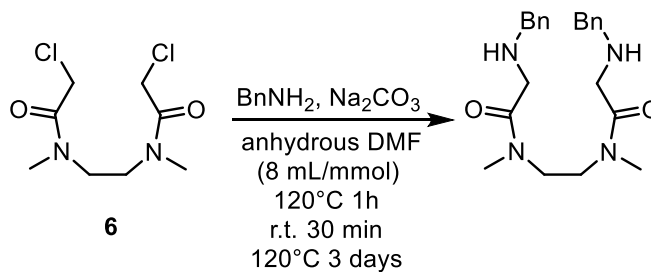
2.1 Alternative Synthesis to Known tacn Derivatives

The synthesis for ^tBu₃tacn from scheme 3 shortcuts the previous method towards other tacn derivatives from 7 steps to 3 steps and doubles the overall yield (~15% to 32%)³⁶. To determine if this synthetic route could be applied for other alkyl derivatives of tacn, ethylene diamine (R=H), *N,N'*-dimethyl ethylene diamine (R=Me), and *N,N'*-dibenzyl ethylene diamine (R=Bn) were subjected to chloro-acetylation, **Scheme 4**.



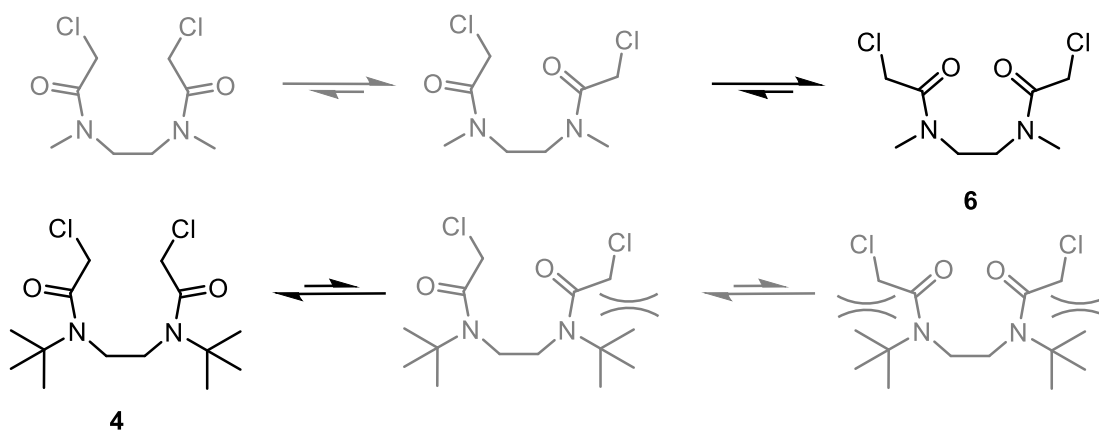
Scheme 4. Chloro-acetylation step

From the ¹H NMR of **6** (R=Me), 2 sets of bridging peaks were observed (see Supporting Information). This phenomenon was first attributed to an impurity in the sample. The “impurity” could not be isolated by column chromatography or recrystallization, so the crude was used for the next step. After cyclization conditions with a primary amine, the linear product, among various polymers, was observed by mass spec (see Supporting Information).



Scheme 5. Attempted cyclization of **6**

Previously reported cyclization with **6** also resulted in low to no yield³⁹. The two sets of peaks in the NMR were revisited. Compound **6** was found to be subject to rotation about the amide bond. These amide rotamers in **Scheme 6** favor different conformers based on steric interactions.



Scheme 6. *Top:* Methyl substituted derivative favor equilibrium to the right. *Bottom:* *Tert*-butyl substituted derivative favor equilibrium to the left due to steric interactions.

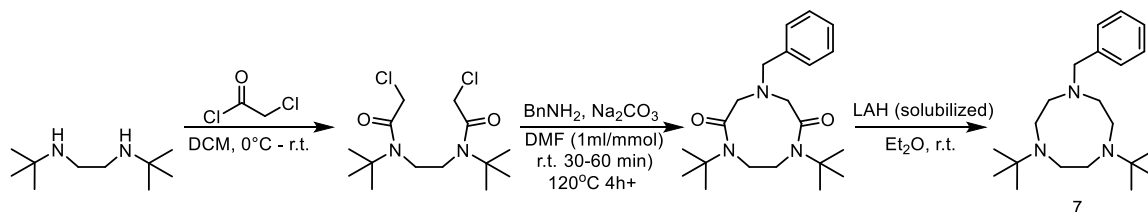
After the addition of a primary amine, **6** will likely yield a linear product, while **4** will likely yield a cyclized product. In conclusion, the synthesis of tBu₃tacn is not a viable synthetic route to Me₃tacn or Bn₃tacn. Focus was then shifted to using **4** and a primary amine to form other derivatives.

2.2 Di- and Mono- *tert*-butyl tacn

In previous unpublished work, Cu(I)tBu₃tacn reacts with atmospheric O₂ to form a dimeric ^s**P**, which could be isolated and crystalized. After subjecting the species to substrates with weak CH bonds and phenolic substrates, the complex was not found to be suitable for a tyrosinase-like oxidative pathway, due to the steric bulk surrounding the copper centers, not allowing a substrate to bind. Percent buried volume calculations

derived from crystal structures supported this reasoning, indicating that the coordination sphere surrounding the copper center is more occupied than previous tacn derivatives.

Opening up this coordination sphere, while still prohibiting α -amino CH bonds, might allow for coordination and oxidation of a substrate. To probe this hypothesis, the amine used in the cyclization step of **Scheme 3** was substituted with different primary amines, which when deprotected, would yield the desired tacn. The selected amine also needed to be nucleophilic enough to substitute both chlorines and cyclize the ring. The first amine screened was benzyl amine. Successfully, benzyl amine could cyclize the ring and the reduction gave **7**, Bn^tBu₃tacn (1-benzyl-1,4-di-*tert*-butyl-1,4,7-triazacyclononane) by **Scheme 7**.



Scheme 7. Synthesis of Bn^tBu₃tacn

This previously inaccessible asymmetric ligand reacted with CoCl₂, and the crystal structure is shown in **Figure 1**. Like ^tBu₃tacn, this ligand enforces 4-coordinate geometry on the cobalt (II) center.

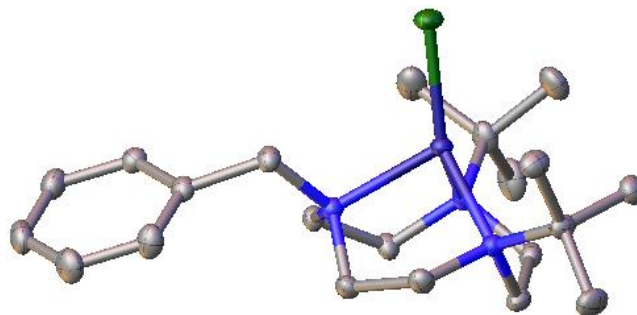


Figure 1. Cobalt complex of $\text{Bn}^t\text{Bu}_3\text{tacn}$ (hydrogens and counter-anion omitted for clarity)

Ligand **7** was subjected to hydrogenation conditions to remove the benzyl group, but only starting material was obtained after the reaction. Other procedures for benzyl deprotection⁴⁰ were tested, but only starting materials were recovered.

In search for a more labile protecting group, trityl was considered. After cyclization conditions of **4** with trityl amine prepared by literature procedure⁴¹, crystalline product was obtained with unexpected ¹H NMR integration. X-ray crystallography, **Figure 2**, confirmed the linear product was formed.

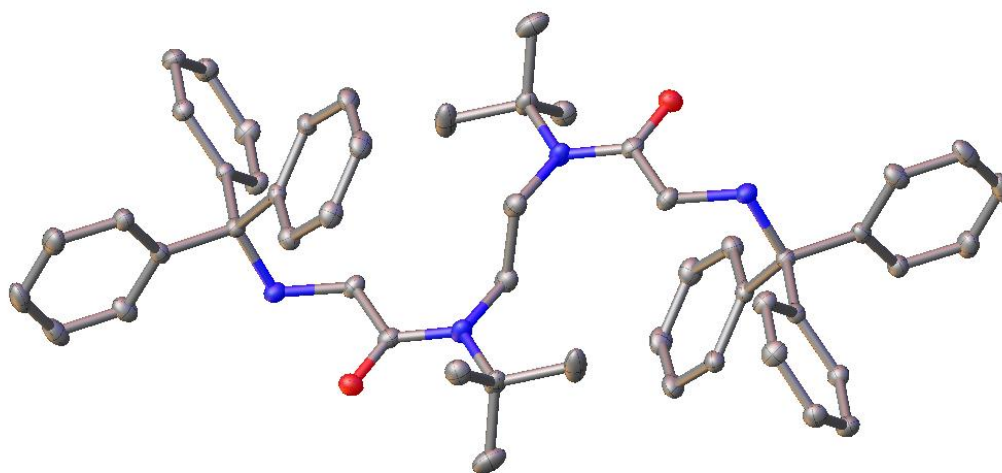


Figure 2. Crystal structure of the linear product formed with trityl amine (hydrogens omitted for clarity)

The steric strain required to cyclize on trityl amine appears to exceed the strain imposed by the *tert*-butyl groups. No further work was done with this ligand or protecting group.

PMB amine (*para*-methoxy benzyl amine), similar to benzyl amine but more easily removed, was then tested to close the ring. After successful cyclization, the PMB group was removed via literature procedure with DDQ (2,3-Dichloro-5,6-dicyano-1,4-benzoquinone)⁴². The compound was subjected to reduction conditions and H^tBu₂tacn (1,4-di-*tert*-butyl-1,4,7-triazacyclononane) was crystallized as an HCl salt in less than 10% yield, **Figure 3**.

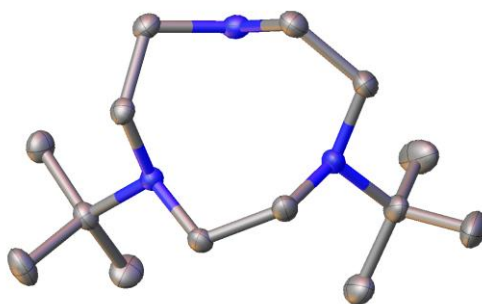


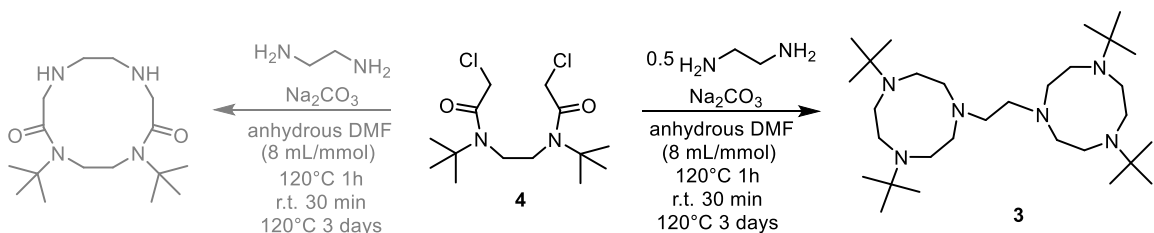
Figure 3. Crystal Structure of H^tBu₂tacn (hydrogens omitted for clarity)

Current efforts have found some success using methanolic NH₃ or NH₄OH under different reaction conditions, eliminating the need for protecting groups to yield H^tBu₂tacn.

In conclusion, cyclization conditions with *tert*-butyl, benzyl, and PMB amine yielded cyclized products, which could be reduced to form their corresponding tacn derivatives. The synthesis of H^tBu₂tacn remained unoptimized and, the limits of the preference to cyclize on one amine were further investigated.

2.3 Bridging tacn Synthesis

The focus of the project became the cyclization step. From the data in **Scheme 4**, structure **4** was in a conformation that favored cyclization. In a representative case, cyclization around EDA (ethylene diamine) was attempted. Two possible cyclized products, shown in **Scheme 8**, were hypothesized based on which amine would close the ring.



Scheme 8. Possible cyclizations with **4** and EDA

As speculated, **4** cyclized around each of the two amines to obtain ligand **3** precursor, which upon reduction, yielded tBu₂dtne (1,2-bis(4,7-di-*tert*-butyl-1,4,7-triazonan-1-yl)ethane) as a crystalline product (**Figure 4**).

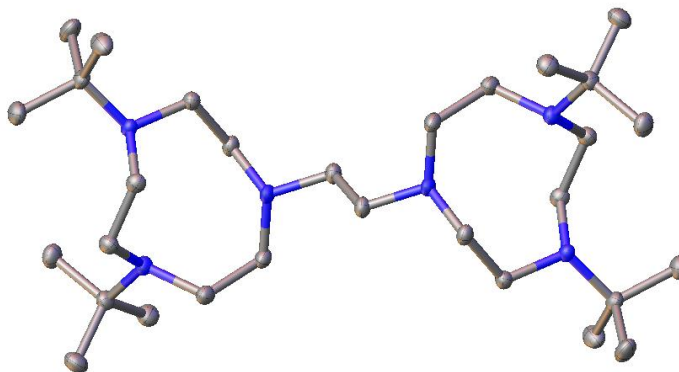


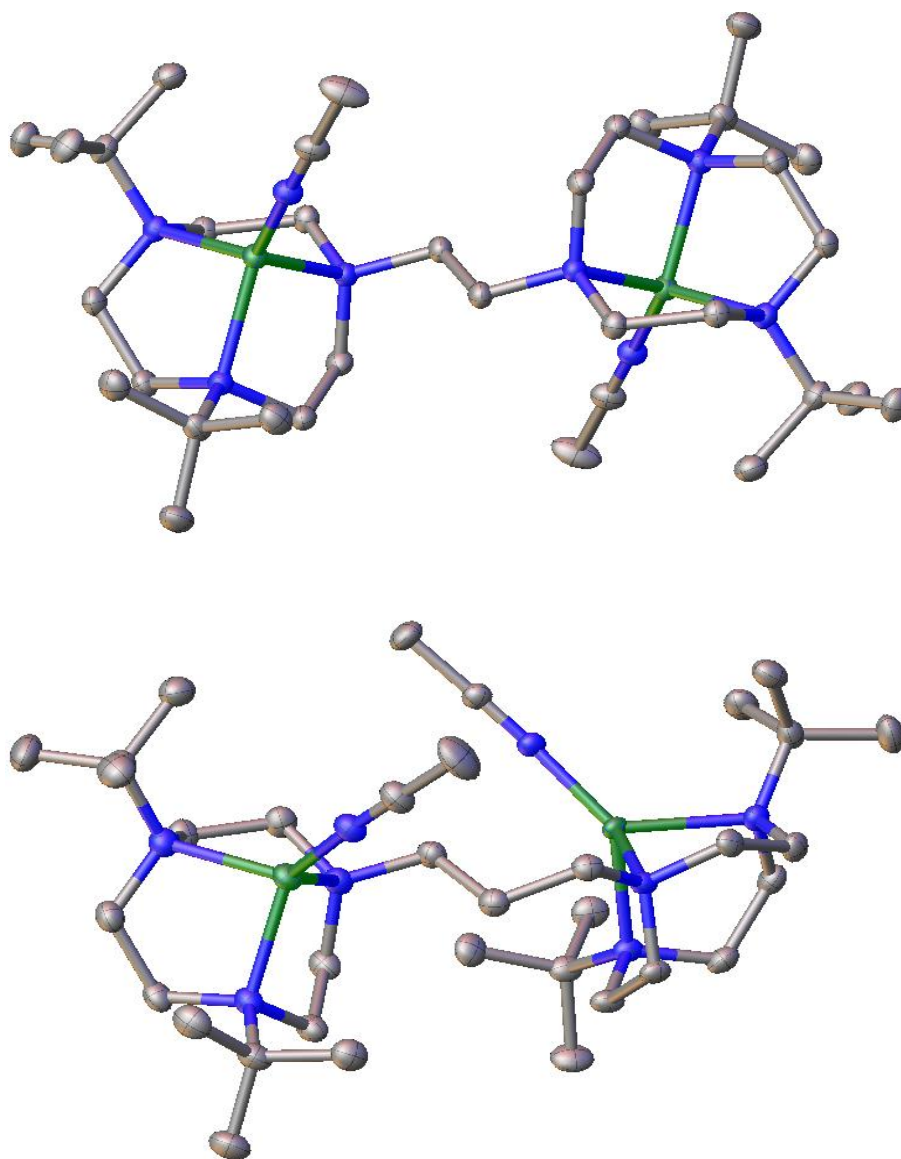
Figure 4. Crystal structure of 1,2-bis(4,7-di-*tert*-butyl-1,4,7-triazonan-1-yl)ethane. (hydrogens omitted for clarity)

The same procedure was carried out with 1,3-diamino-propane as the primary amine, and tBu₂dtnp (1,2-bis(4,7-di-*tert*-butyl-1,4,7-triazolan-1-yl)propane), the corresponding propyl bridged tacn, was obtained in moderate yields, but could not be crystallized. From these ligands, metal complexes could be formed and their reactivity determined.

2.4 Bridging Copper tacn Complexes

Copper (I) complexes of the tBu₂dtne and tBu₂dtnp were prepared in an air- and moisture-free environment. These complexes were crystallized by vapor diffusion with methylene chloride and ether to afford the crystal structures shown in **Chart 4** with some red solids, as evidence of disproportionation.

Chart 4. *Top:* Crystal Structure of $\text{Cu(I)-}^t\text{Bu}_2\text{dtne}(\text{MeCN})_2(\text{PF}_6)_2$ *Bottom:* Crystal Structure of $\text{Cu(I)-}^t\text{Bu}_2\text{dtnp}(\text{MeCN})_2(\text{PF}_6)_2$ (hydrogens and counter-anions omitted for clarity)



Upon exposure to air, both of the pale yellow solutions of the complexes in DCM, benzene, or MeCN turned brown. After a few hours the solutions became green. The species formed by the $\text{Cu(I)-}^t\text{Bu}_2\text{dtne}$ after exposed to air was crystallized by vapor diffusion. The crystal was highly twinned, but a rough connectivity was solved, **Figure 5**.

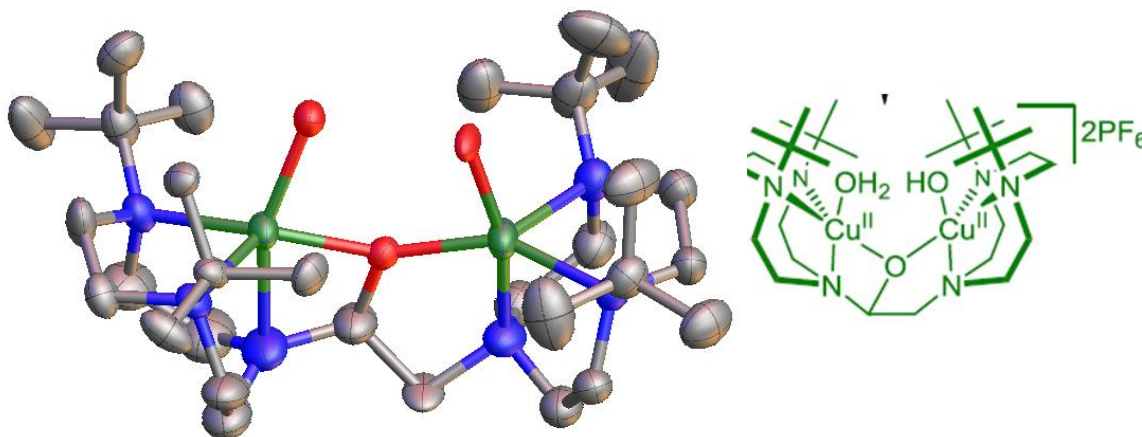


Figure 5. Crystal Structure and ChemDraw of Cu-¹Bu₂dtne (MeCN)₂ (PF₆)₂ after O₂ exposure (hydrogens and counter-anions omitted for clarity)

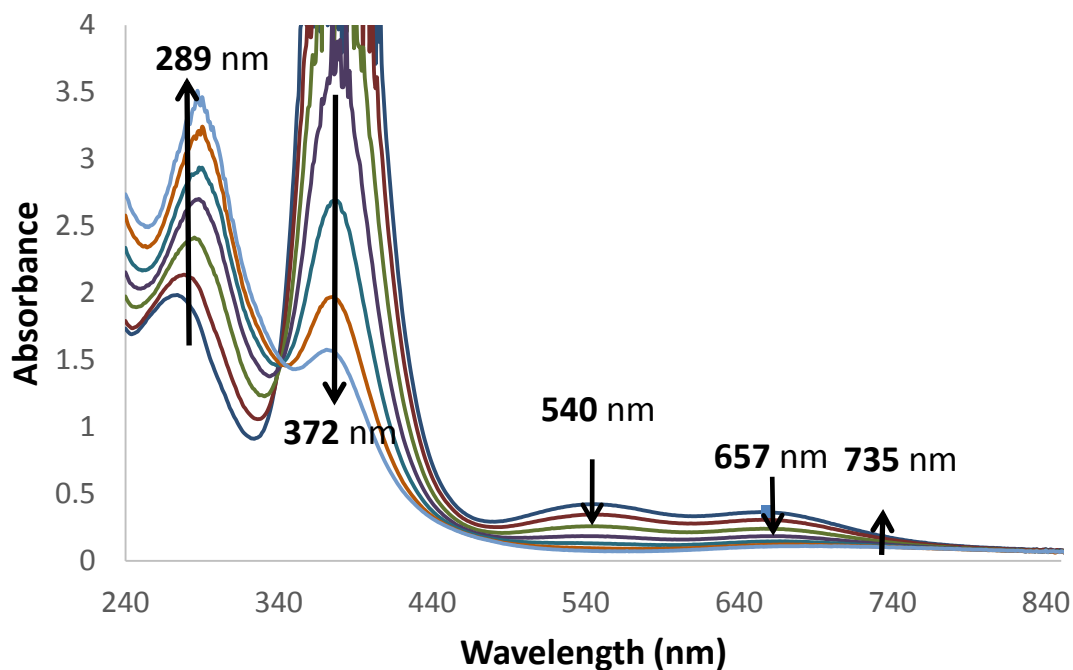
The Cu/O₂ complex appears to have activated the CH bond on the ligand bridge, and picked up a water molecule. Extraction of the ligand was attempted with NH₄OH; however, the ¹H NMR spectrum was always saturated with broad signals. Extraction was expected to cleave the ethane bridge, resulting in two separate tacn units. For comparison, **reaction ii** in **Chart 3**, CH activation occurred on the isopropyl group and not the bridging ethane. Since the above complex has *tert*-butyl substituents, the weakest CH bond was on the ethane bridge.

Attempts at recrystallizing the oxidized form of Cu₂-¹Bu₂dtnp failed. Most likely the dioxygen intermediate reacts with the bridging ligand to yield a structure similar to the oxidized Cu₂-¹Bu₂dtne. Because there are CH bonds which are symmetrically inequivalent, mixtures of the two forms could prevent crystallization.

To probe the decomposition intermediates the reaction with O₂ was monitored by UV-vis at -40 °C at 30-minute intervals. The Cu(I)₂-¹Bu₂dtne dissolved in DCM was initially featureless. Upon exposure to O₂, an intense charge transfer band grew in the high energy region and two weaker features in the visible/near IR. The 372, 540, and 657

nm bands intensified to a maximum value, then decomposed to a moderately intense feature at 289 and a comparatively weak feature at 735 nm giving rise to the green color (Chart 5).

Chart 5. Cu-^tBu₂dtne(MeCN)₂(PF₆)₂ at -40 °C 3-6 hours after exposure to O₂



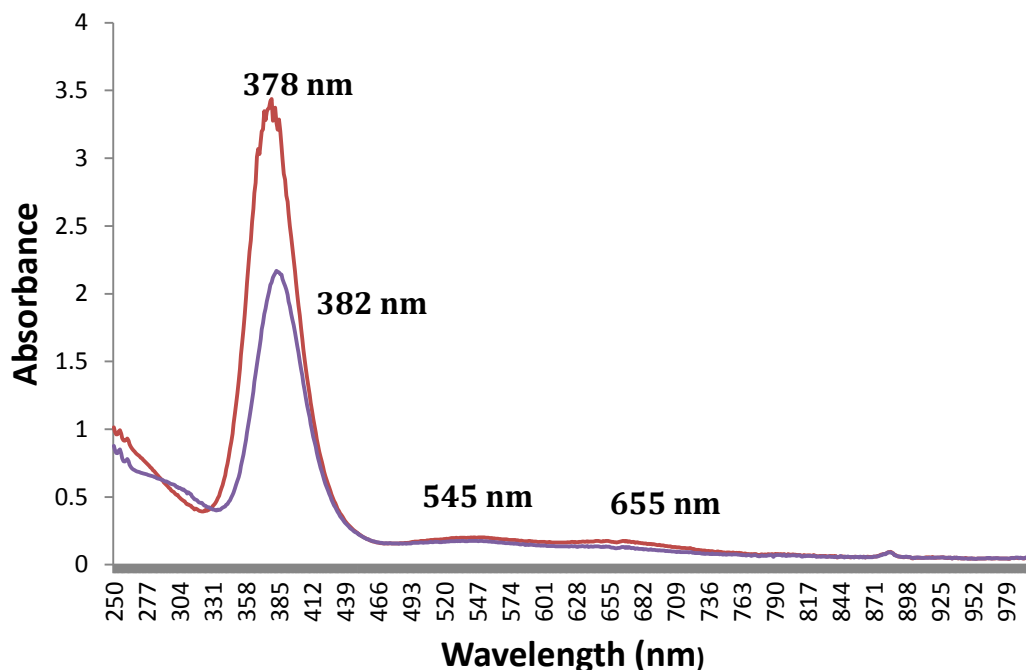
When Cu(OTf) benzene salt was used in place of the [Cu(MeCN)₄]PF₆ salt the peaks of the oxygenated product ligated with ^tBu₂dtne remained unchanged, suggesting the MeCN in the PF₆ salt no longer coordinates to the coppers in the observed intermediate.

Based on the data in **Table 1**, the observed intermediate could potentially be in **SO** or **^{m3}O** binding mode. The distinction between transitions assigned to these two binding modes has historically been unclear in the literature. Furthermore, the intermediate is likely not a combination of any modes presented in the table, as evidenced by the number and position of transitions and the isosbestic point at 340nm. Further

experiments, like resonance Raman, would distinguish between the two possible structures.

A similar O₂ experiment was conducted with Cu(I)-^tBu₂dtne(OTf)₂ and Cu(I)-^tBu₂dtne (OTf)₂. The UV-vis spectra are shown in **Chart 6**.

Chart 6. Overlay UV-vis spectra of Cu-^tBu₂dtne(OTf)₂ in red and Cu-^tBu₂dtnp(OTf)₂ in purple in DCM 5 minutes after exposure to air



Nearly identical features appear with both ligands. A noticeable difference, however, is the ratio of peak intensities. The difference suggests torsional strain about the Cu-O-O-Cu bonds that is relieved by the more flexible propyl bridged ^tBu₂dtnp.

To conclude, ^tBu₂dtne and ^tBu₂dtnp are capable of forming copper complexes which can activate atmospheric oxygen. Like other literature precedented systems, these complexes undergo ligand degradation at room temperature. Future work is aimed at better understanding these systems and modifying the structure to achieve catalytic oxidation under ambient conditions.

3.0 Future Studies

3.1 Spectroscopic Studies

In the future, resonance Raman data would elucidate the Cu/O₂ binding modes in the intermediate steps. The Raman peaks for the modes are more unique to the core structure (and better defined in the literature) than the electronic transitions. Also, SQUID experiments would elucidate the coupling between the copper cores and whether the intermediate species is anti-ferromagnetically coupled or ferromagnetically coupled. This data would provide information on the torsion of the Cu-O-O-Cu bond⁴³.

However, the most definitive structure analysis would be X-ray crystallography. There are examples in the literature of Cu/O₂ adducts crystallized at low temperatures. The copper (I) complex would first need to be cooled to -40 to -80 °C, and then the addition of O₂ at low temperature might form crystals after several days, according to previous literature procedures⁴³.

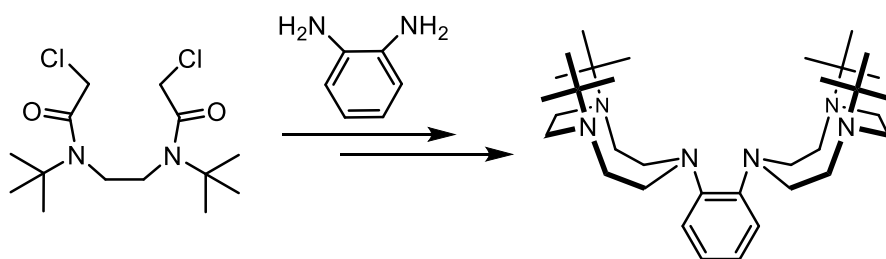
Additionally lifetime studies and determination of absorptivity would better complete the characterization of the tBu₂dtne copper complex, but would only serve as a comparison to the other systems that have been documented¹⁶.

3.2 New Bridging Ligands

Since the Cu₂/O₂ core oxidizes the weak CH bonds on the ethyl- and propyl- bridged ligands, protection at these positions might favor an active species capable of intermolecular oxidation under ambient conditions. Two possible modes of protection are the incorporation of an aromatic ring, or the addition of methyl groups.

3.2.1 Aryl- Bridging Unit

An aryl bridged species would be particularly attractive because the rigidity of the phenyl ring forces the two nucleation sites to point towards each other, unlike dtne (**Chart 4 top**) where the nucleation sites point away. Karlin and coworkers have observed H-atom abstraction when using a dinuclear copper compound with a meta-substituted bridge⁴⁴. An ortho-substituted bridge (**Scheme 9**) would remove the active CH bond in close proximity to the active site in his complex.



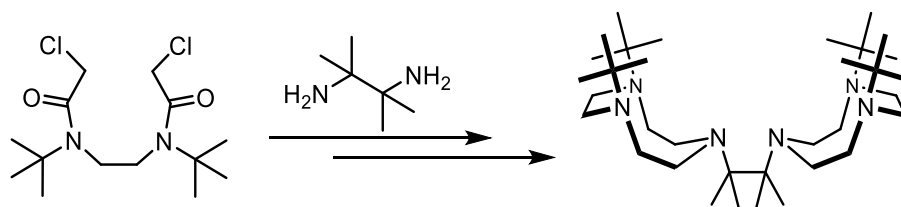
Scheme 9. Target aryl-bridged ligand

Preliminary results, however, show that cyclization with *o*-phenylene diamine does not result in any product. The steric environment around the ortho-amines might be too great, though the desired product may be favorable under a different set of reaction conditions.

3.2.2 Methyl-Protected Bridging Unit

Another method to protect the bridging unit would be replacing the CH bonds with methyl groups. To preserve the synthetic route, a gem-dimethyl diamine must be used for the cyclization reaction. 2,3-Diamino-2,3-dimethyl propane can be prepared

according to a modified literature procedure⁴⁵. The diamine was subjected to cyclization conditions, **Scheme 10**.



Scheme 10. Target methyl protected ethane bridge

Though the crude TLC separates at least 4 different products, mass spec suggests that the bridging dione species is present coordinating protonated water, as well as the singly cyclized product.

4.0 Conclusions

Oxidation reactions are relevant to industry, biochemistry, and organic synthesis. These reactions are performed in industry with the aid of high temperature and pressure, often with an expensive second-/third- row transition metal or an inorganic oxidant. Biological systems use abundant first-row metals and atmospheric oxygen to perform similar oxidations. Chemists seek to replicate these transformations with an analogous molecular system.

With some success, oxidation catalysts have been developed using copper. However, these systems can only function at low temperatures because they are subject to ligand oxidation. The tacn derivatives in particular undergo CH activation α to the amine. Previous work from the Scarborough lab has allowed for the development of novel tacn derivatives with tertiary alkyl substituents to remove the activated CH bond.

In this report, the synthesis of $^t\text{Bu}_3\text{tacn}$ has been extended to asymmetric derivatives. Due to the steric bulk of the *tert*-butyl groups, the proximity of the two C-Cl anti-bonding region has been exploited in cyclization to afford bridging tacn species. Copper complexes of these bridging species have the ability to activate atmospheric oxygen. At room temperature, the bridging unit is oxidized.

Future studies will fully characterize the oxidative pathway towards ligand degradation. The bridging unit will also incorporate alkyl or aryl protecting groups to promote intermolecular oxidation.

5.0 Experimental

5.1 General Considerations

Reagents were purchased from either Sigma Aldrich or Strem Chemicals and used as received, unless otherwise noted. *N,N'*-di-*tert*-butylethylenediamine was opened in an air- and moisture-free environment and dried over molecular sieves. Cu(I)OTf benzene complex was purified by dissolving an amount in benzene and heating to 80 °C until all the solids dissolved. The solution was filtered and the solvent was removed to afford a white powder used for metalation. All metalation reactions were performed inside an MBRAUN UNIlab 2000 inert-atmosphere glovebox. All anhydrous solvents were purified and dried by an MBRAUN solvent purification system (SPS). ¹H and ¹³C NMR spectra were recorded at room temperature on Varian 300 or 400 MHz NMR spectrometer. UV–vis/NIR absorption spectra were recorded on a Shimadzu UV-3600 spectrophotometer. Mass spectra were obtained from the Mass Spectrometry Center at Emory University. X-ray crystallographic data were collected on a Bruker Smart 1000 CCD diffractometer in the X-ray Crystallography Laboratory at Emory University.

5.2 Ligand Syntheses

5.2.1 Chloro-acetylation

Representative Procedure for Chloro-acetylation. The following procedure was modified from the literature⁴⁶. Dry methylene chloride was added to an oven-dried 250 mL round-bottom flask. 2-Chloroacetyl chloride was added under nitrogen. The solution was cooled in an ice bath. The corresponding diamine was added via syringe pump over 20 minutes. After, the reaction was allowed to warm to room temperature and the

colorless solution became light yellow. The solution stirred overnight and became turbid. The crude mixture was transferred to a separatory funnel and distilled water (50 mL) was added. Saturated aqueous K_2CO_3 (25 mL) was slowly added to quench the reaction. The mixture was allowed to sit until the turbid layer became translucent (about 30 min). The organic layer was extracted with methylene chloride, washed with brine (3 x 100 mL), and dried over $MgSO_4$. The solution was concentrated under low pressure on the rotary evaporator to afford a pale brown solid. Re-crystallization of the crude from methylene chloride and pentane afforded pure product.

Synthesis of *N,N'*-Bis(2-chloroacetyl)-*N,N'*-di-*tert*butylethylenediamine (4).

Methylene chloride (75mL), 2-chloroacetyl chloride (11mL, 139.1 mmol, 3 eq), *N,N'*-di-*tert*-butylethylenediamine (10mL, 46.4 mmol, 1eq) . The crude product was sufficiently pure to proceed. To isolate the product, crystallization of the crude from methylene chloride and hexane afforded pure product⁴⁶ in 87% isolated yield.

Synthesis of *N,N'*-Bis(2-chloroacetyl)-*N,N'*-dimethyl-ethylene-diamine (6).

Methylene chloride (50 mL), 2-chloroacetyl chloride (3.25 mL, 40.9 mmol, 2.2 eq), *N,N'*-di-methylethylenediamine (2 mL, 18.6 mmol, 1eq). Isolated yield 36% as a mixture of amide rotamers. 1H NMR (300 MHz, $CDCl_3$): δ 4.12, 4.06, 4.03(s, 2H), 3.59, 3.53(s, 2H), 3.13, 3.10, 3.00(s, 3H).

5.2.2 Cyclizations

Representative Cyclization Conditions. The following procedure was modified from the literature⁴⁶. In a vial with a stir bar, **4**, Na₂CO₃, and the corresponding amine or diamine was combined in DMF (1-8 mmol/mL). If anhydrous DMF was used, round-bottom flasks were oven-dried; otherwise vials were used. The mixture was allowed to stir at room temperature for 1-8 hours and heated to 120 °C for 2-72 hours. After cooling, distilled H₂O was added and the organic layer was extracted with DCM 3 times. The organic layer was washed with brine 5 times, dried on Na₂SO₄, filtered, and concentrated on the rotary evaporator. The crude was recrystallized with DCM/pentanes, unless otherwise noted.

Synthesis of 1,4-Di-*tert*-butyl-7-benzyl-1,4,7-triazocyclononane-2,6-dione. NaCO₃ (8.86 g, 84.46 mmol, 2.5 eq), **4** (11.0g, 33.78 mmol, 1eq), Benzylamine (4.06mL, 37.16mmol, 1.1 eq), 450 mL anhydrous DMF. Stir 1 hr at room temperature. Stir 72 hours at 120°C. Isolated Yield: 36%. ¹H NMR (300 MHz, CDCl₃): δ 7.34(m, 5H), 3.85(s, 2H), 3.74(s, 4H), 3.47(s, 4H), 1.42(s, 18H). ESI-MS (m/z): calculated for {C₂₁H₅₃N₂O₂N₃ + H⁺}, 360.26455; found, 360.26402 (Δ = 1.47ppm)

Synthesis of *N,N'*-diaminobenzyl-3,8-diacetyl-4,7-dimethyl-ethylene-diamine. NaCO₃ (1.1 g, 10.4 mmol, 2.5 eq), **6** (1.0g, 4.16 mmol, 1eq), Benzylamine (0.5mL, 4.56mmol, 1 eq), 40 mL anhydrous DMF. Stir 1 hr at room temperature. Stir 72 hours at 120°C. ESI-MS (m/z): calculated for {C₂₂H₃₀N₄O₂Cl₂ + H⁺}, 383.24415; found, 383.24390(Δ = 0.66 ppm)

Synthesis of *N,N'*-diaminotrityl-3,8-diacetyl-4,7-di-*tert*-butyl-ethylene-diamine. 4 (2.0g, 6.15 mmol, 1eq), NaCO₃ (1.613 g, 15.37 mmol, 2.5 eq), Tritylamine⁴¹ (1.75g, 6.76mmol, 1.1 eq), 65 mL anhydrous DMF. Stir 1 hr at room temperature. Stir 72 hours at 120°C. ¹H NMR (300 MHz, CDCl₃): δ 7.44(d, 4H), 7.18(m, 6H), 3.33(t, 3H, 5.4Hz), 3.19(d, 6H, 5.1Hz), 2.89(s, 4H) , 1.57(s, 18H). ESI-MS (m/z): calculated for {C₃₅H₄₈N₄O₂ + H⁺}, 557.38500; found, 557.38396 (Δ = 1.87 ppm).

Synthesis of 1,4-Di-*tert*-butyl-7(4-methoxy-benzyl)-1,4,7-triazoclononane-2,6-dione. 4 (2.0g, 6.15 mmol, 1eq), NaCO₃ (1.613 g, 15.37 mmol, 2.5 eq), 4-Methoxybenzylamine (0.88mL, 6.76mmol, 1.1 eq), 65 mL anhydrous DMF. Stir 1 hr at room temperature. Stir 72 hours at 120°C. Yield: 68%. ¹H NMR (300 MHz, CDCl₃): δ 7.28(d, 2H, 8.4Hz), 6.87(d, 2H, 8.4Hz), 3.80(s, 3H), 3.77(s, 6H) , 3.46(s, 4H) , 1.44(s, 18H). ESI-MS (m/z): calculated for {C₂₂H₃₅N₃O₃ + H⁺}, 390.27512; found, 390.27525 (Δ = 0.34ppm)

Synthesis of 1,2-bis(4,7-di-*tert*-butyl-1,4,7-triazonan-1-yl)-2,6-dioxo-ethane. 4 (2.0g, 6.15 mmol, 2.1eq), NaCO₃ (1.29 g, 12.30 mmol, 4 eq), Ethylene diamine (0.21mL, 3.07mmol, 1 eq), 8 mL DMF. Stir 1 hr at room temperature. Stir 2 hours at 120 °C. Yield 69%. ¹H NMR (400 MHz, CDCl₃): δ 3.69(s, 4H), 3.49(s, 4H), 2.86(s, 2H), 1.41(s, 18H). ¹³C NMR (100 MHz, CDCl₃): δ 171.55, 60.29, 57.79, 52.52, 48.26, 29.06. ESI-MS (m/z): calculated for {C₃₀H₅₆N₆O₄ + H⁺}, 565.44358; found, 565.44368(Δ = 0.18 ppm)

Synthesis of 1,2-bis(4,7-di-*tert*-butyl-1,4,7-triazonan-1-yl)-2,6-dioxo-propane. 4 (2.0g, 6.15 mmol, 2.1eq), NaCO₃ (1.29 g, 12.30 mmol, 4 eq), 1,3diamino-propane (0.26mL, 3.07mmol, 1 eq), 8 mL DMF. Stir 1 hr at room temperature. Stir 2 hours at 120°C. Yield 50%. ¹H NMR (400 MHz, CDCl₃): δ 3.73(s, 8H), 3.44(s, 8H), 2.64(t, 4H, 7.2Hz), 1.78(quin, 2H, ~4.5Hz), 1.41(s, 36H).

5.2.3 Oxidation/Reductions

Synthesis of 1,4-Di-*tert*-butyl-1,4,7-triazocyclononane-2,6-dione. In a round-bottom flask, 1,4-Di-*tert*-butyl-7(4-methoxy-benzyl)-1,4,7-triazocyclononane-2,6-dione (2.3g, 5.88 mmol, 1 eq) and DDQ (2.0 g, 8.84 mmol, 1.5 eq) were combined in a mixture of 200mL of methylene chloride and 20 mL of water. The dark mixture stirred for 2 hours at room temperature. The organic layer was extracted with aqueous NaHCO₃ and DCM. The organic layer was washed with brine, dried over MgSO₄, filtered, and concentrated on the rotary evaporator. The crude mixture was columned with EtOAc with 10% MeOH and 1% TEA on silica gel (Rf= 0.55). An accurate yield could not be obtained because the product was red, indicating that the solid contained the ¹H-NMR silent product of the reacted DDQ. The maximum yield by weight was 43%. ¹H NMR (300 MHz, CDCl₃): δ 3.18(s, 4H), 3.58(s, 4H), 1.46(s, 18H). ESI-MS (m/z): calculated for {2x(C₁₄H₂₆N₃O₂) + H⁺}, 539.42793; found, 539.42775(Δ = 0.33ppm).

Representative Procedure for Amide Reduction. *CAUTION: LiAlH₄ violently reacts with water and should be handled appropriately.* The following procedure was modified from the literature⁴⁶. In the glovebox, impure lithium aluminum hydride (5 eq-15eq) was

dissolved in dry ether and stirred overnight. The mixture was filtered over Celite into a round-bottom flask with a stir bar. The solids were suspended in dry ether and carefully quenched with isopropanol before being discarded. The amide was dissolved in dry ether and slowly added to the clear filtrate. The mixture stirred overnight. The colorless mixture was removed from the glovebox and quenched in the following order: 1 eq. distilled H₂O (relative to grams LAH used), 2 eq. 10% NaOH, 3 eq. H₂O. The mixture was allowed to stir for 1 hour to ensure the excess LiAlH₄ was quenched. The reaction mixture was filtered and washed with THF. The organic layer was dried with Na₂SO₄ and concentrated under reduced pressure. The product was crystallized from hot EtOH unless otherwise noted.

Synthesis of 1,4-di-*tert*-butyl-1,4,7-triazacyclononane. LiAlH₄ (2.18 g, 57.37 mmol, 5.22eq), 1,4-Di-*tert*-butyl-1,4,7-triazacyclononane-2,6-dione (2.96g, 10.99mmol, 1eq). The resulting oil was acid/base extracted and the product crystallized from EtOH/H₂O. Isolated yield <10% as HCl salt. ¹H NMR (300 MHz, CDCl₃): δ 3.02(t, 4H, 5.7Hz), 2.77(t, 4H, 6.0Hz), 2.61(s, 4H), 1.11(s, 18H).

Synthesis of 1,4-di-*tert*-butyl-7-benzyl-1,4,7-triazacyclononane. LiAlH₄ (4.46g, 117.5 mmol, 9eq), 1,4-Di-*tert*-butyl-7-benzyl-1,4,7-triazacyclononane-2,6-dione (4.33g, 13.06 mmol, 1eq). Yield:80%. ¹H NMR (300 MHz, CDCl₃): δ 7.40(d, 2H), 7.31(d, 2H), 7.21(t, 1H), 3.67(s, 2H), 2.93(t, 4H), 2.64(s, 8H), 1.04(s, 18H).

Synthesis of 1,2-bis(4,7-di-*tert*-butyl-1,4,7-triazonan-1-yl)ethane. LiAlH₄(1.01 g, 26.53 mmol, 15eq), 1,2-bis(4,7-di-*tert*-butyl-1,4,7-triazonan-1-yl)-2,6-dioxo-ethane (1, 1.77, 1eq), 30 mL ether. Isolated yield: 58%. ¹H NMR (300 MHz, CDCl₃): δ 2.97(t, 8H, 4.2Hz), 2.67(t, 8H, 4.5Hz), 2.62(s, 8H), 1.83(s, 4H), 1.03(s, 36H). ¹³C NMR (100 MHz, CDCl₃): δ 55.96, 55.56, 54.86, 52.79, 50.26, 26.93.

Synthesis of 1,2-bis(4,7-di-*tert*-butyl-1,4,7-triazonan-1-yl)propane. LiAlH₄(1.01 g, 26.53 mmol, 15eq), 1,2-bis(4,7-di-*tert*-butyl-1,4,7-triazonan-1-yl)-2,6-dioxo-propane (1, 1.77, 1eq), 30 mL ether. Isolated yield: 42%. ¹H NMR (300 MHz, CDCl₃): δ 2.97(t, 8H, 4.5Hz), 2.67(t, 8H, 4.5Hz), 2.59(s, 8H), 2.50(t, 4H, 7.5Hz), 1.61(quint, 2H, 4.5Hz), 1.04(s, 36H).

5.3 Metal Complexes

Synthesis of Cobalt (I) 1,4-di-*tert*-butyl-7-benzyl-1,4,7-triazacyclononane Cl. In the glovebox, 1,4-di-*tert*-butyl-7-benzyl-1,4,7-triazacyclononane (100 mg), anhydrous CoCl₂ (39 mg), and sodium tetraphenylborate (300 mg, 3eq) were combined in 15 mL of MeCN. The mixture stirred overnight, then filtered over Celite. The solvent of the filtrate was removed. Dark blue crystals were obtained by layering the MeCN with ether.

Representative Procedure for Copper(I) BF₄ and PF₆ Salts. In the glovebox, the binucleating tacn ligand (100 mg, 1eq) and copper acetonitrile salt (2 eq) were combined in 3mL of MeCN. The solution was stirred overnight, and then filtered over Celite. After the solvent was removed, crystals were obtained by vapor diffusion either with

DCM/pentanes or MeCN/ether. When DCM was used, unidentified red solids were also obtained.

Representative Procedure for Copper (I) (CF_3SO_3) Salts. In the glovebox, the tacn ligand (50 mg, 1eq) and purified Cu (I) triflate benzene (2eq) were combined in 5mL of benzene. The mixture was shaken until most solids dissolved and allowed to sit overnight. The reaction mixture was decanted and the solids dried. The resulting off-white powder was used for spectroscopic experiments.

6.0 Supporting Information

6.1 NMR

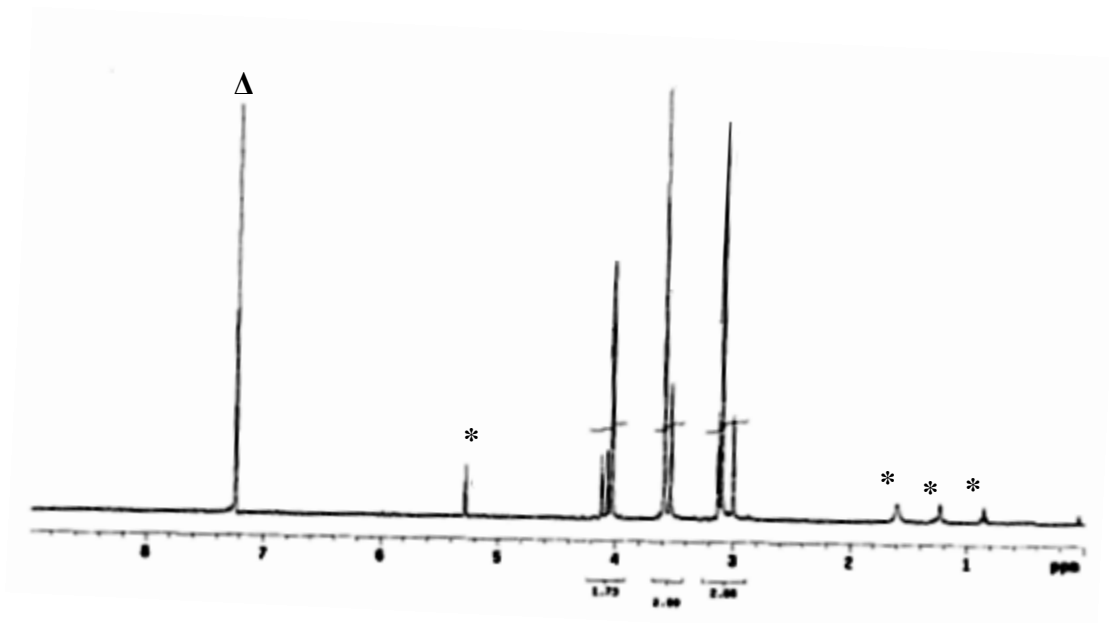


Chart 7. ¹H NMR of *N,N'*-Bis(2-chloroacetyl)-*N,N'*-dimethyl-ethylene-diamine (6). Sets of peaks identified as amide rotamers. (* impurities, Δ solvent)

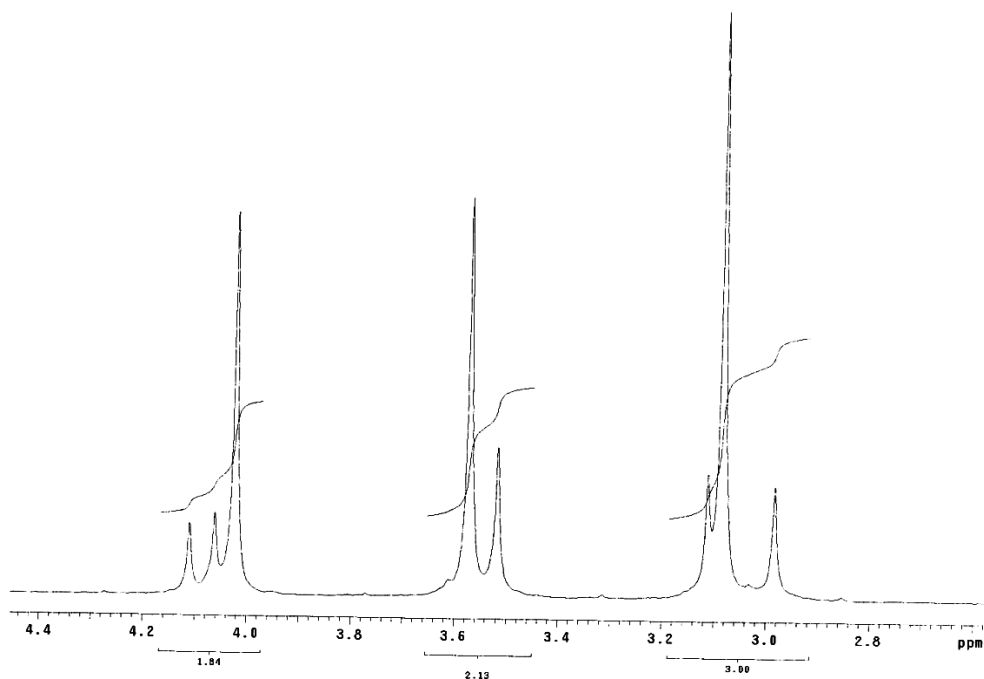


Chart 8. Rotamer region ¹H NMR of *N,N'*-Bis(2-chloroacetyl)-*N,N'*-dimethyl-ethylene-diamine (6)

6.2 Mass Spec

FT24404_130806121241 #80-88 RT: 1.45-1.58 AV: 9 NL: 1.85E6
T: FTMS + p NSI Full ms [100.00-1000.00]

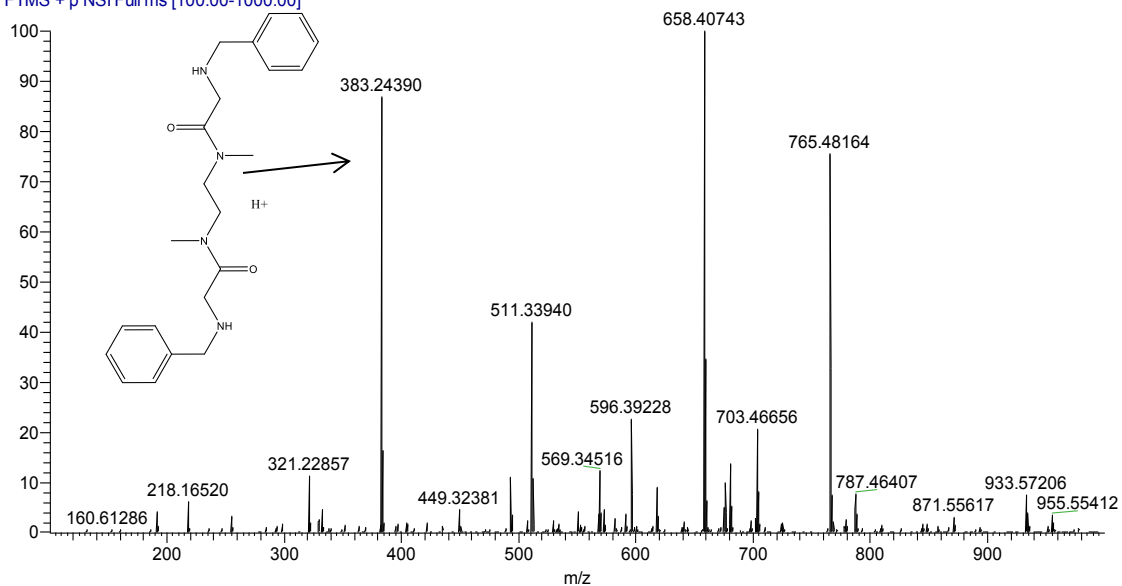


Chart 9. Mass spec of polymerized product of *N,N'*-Bis(2-chloroacetyl)-*N,N'*-di-methylene-diamine with benzyl amine

FT27982_150212134740 #32-38 RT: 0.51-0.60 AV: 7 NL: 2.09E7
T: FTMS + p NSI Full ms [100.00-700.00]

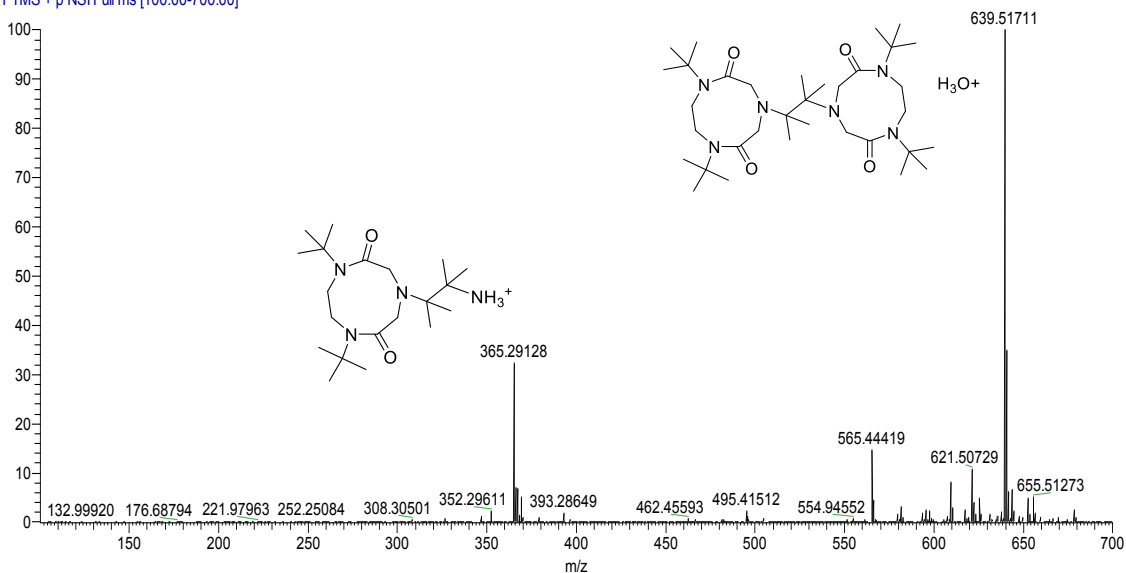


Chart 10. Preliminary mass spec result for 2,3-bis(4,7-di-*tert*-butyl-1,4,7-triazonan-1-yl)-2,6-dione)-2,3-dimethyl-propane

6.3 UV-Vis Spectra

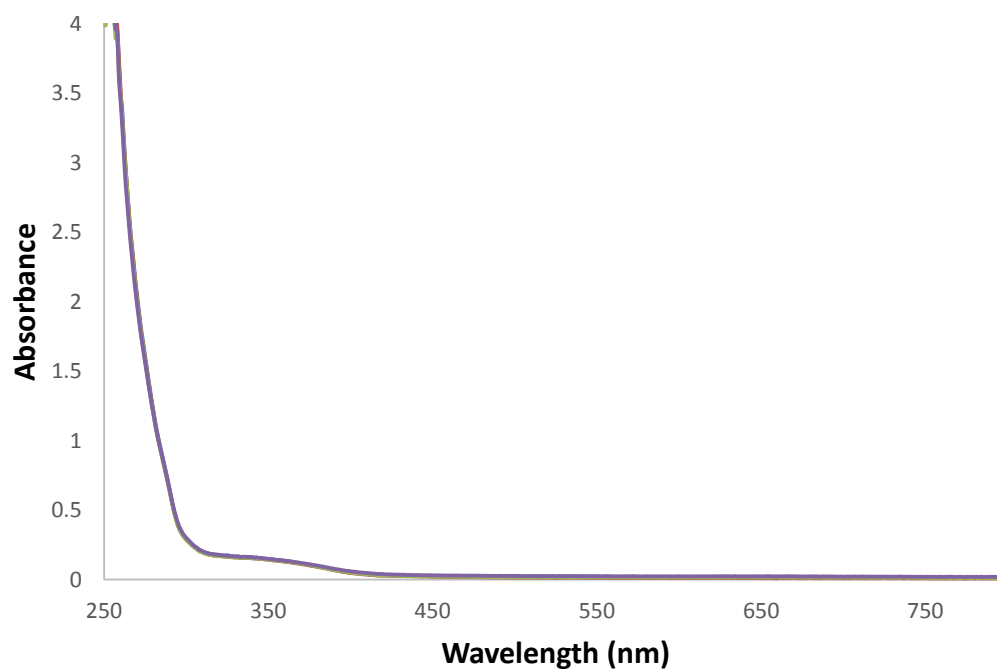


Chart 11. UV-vis of $\text{Cu(I)-}^t\text{Bu}_2\text{dtne(MeCN)}_2\text{PF}_6$ before exposure to O_2

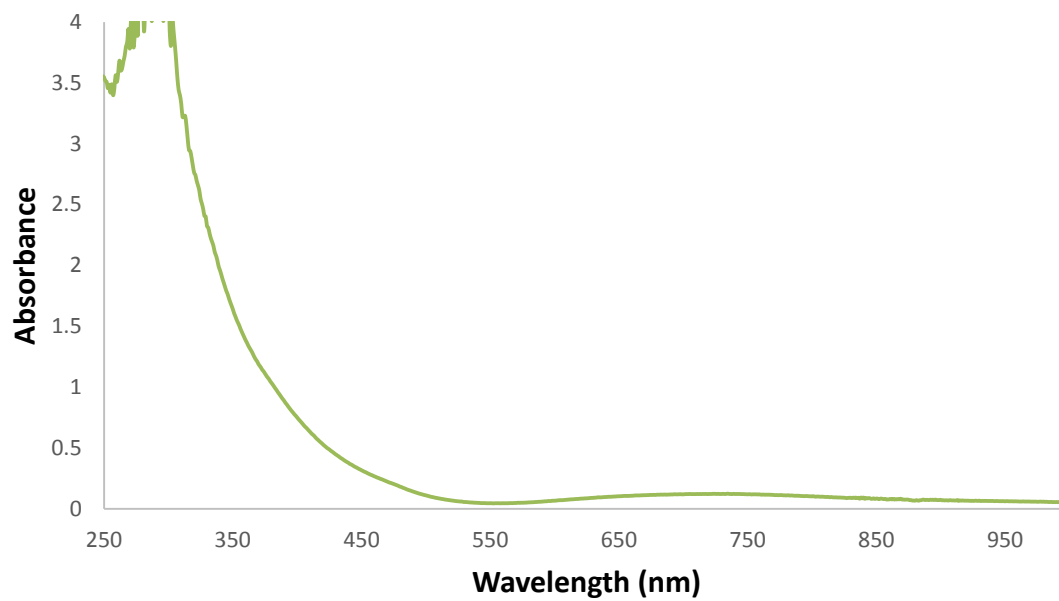


Chart 12. UV-vis of $\text{Cu-}^t\text{Bu}_2\text{dtne}$ final product after exposure to O_2

6.4 Crystallographic Data

Table 2. Crystal Data for Cobalt (I) 1,4-di-*tert*-butyl-7-benzyl-1,4,7-triazacyclononane Cl (Figure 1)

Empirical formula	C ₄₇ H ₆₀ BClCoN ₄
Formula weight	786.18
Temperature/K	109.01
Crystal system	triclinic
Space group	P-1
a/Å	11.3644(7)
b/Å	13.2093(8)
c/Å	15.5446(10)
α/°	75.1860(9)
β/°	72.2525(10)
γ/°	73.5160(10)
Volume/Å ³	2094.2(2)
Z	2
ρ _{calc} /g/cm ³	1.247
μ/mm ⁻¹	0.511
F(000)	838.0
Crystal size/mm ³	0.57 × 0.326 × 0.315
Radiation	MoKα (λ = 0.71073)
2θ range for data collection/°	3.86 to 66.188
Index ranges	-17 ≤ h ≤ 17, -20 ≤ k ≤ 20, -23 ≤ l ≤ 23
Reflections collected	36136
Independent reflections	14862 [R _{int} = 0.0323, R _{sigma} = 0.0435]
Data/restraints/parameters	14862/0/494
Goodness-of-fit on F ²	1.043
Final R indexes [I ≥ 2σ (I)]	R ₁ = 0.0497, wR ₂ = 0.1294
Final R indexes [all data]	R ₁ = 0.0623, wR ₂ = 0.1374
Largest diff. peak/hole / e Å ⁻³	0.97/-0.45

Table 3. Crystal Data for *N,N'*-diaminotriptyl-3,8-diacetyl-4,7-di-*tert*-butyl-ethylene-diamine (Figure 2)

Empirical formula	C ₅₂ H ₅₈ N ₄ O ₂
Formula weight	771.02
Temperature/K	110(2)
Crystal system	triclinic
Space group	P-1
a/Å	8.8769(7)
b/Å	10.5221(8)
c/Å	13.1136(10)
α/°	109.0912(9)
β/°	109.3679(9)
γ/°	95.5584(9)
Volume/Å ³	1062.63(14)
Z	1
ρ _{calc} /cm ³	1.205
μ/mm ⁻¹	0.073
F(000)	414.0
Crystal size/mm ³	0.703 × 0.327 × 0.134
Radiation	MoKα (λ = 0.71073)
2θ range for data collection/°	4.21 to 62.13
Index ranges	-12 ≤ h ≤ 12, -15 ≤ k ≤ 15, -19 ≤ l ≤ 19
Reflections collected	20615
Independent reflections	6767 [R _{int} = 0.0256, R _{sigma} = 0.0279]
Data/restraints/parameters	6767/0/269
Goodness-of-fit on F ²	1.040
Final R indexes [I ≥ 2σ (I)]	R ₁ = 0.0521, wR ₂ = 0.1386
Final R indexes [all data]	R ₁ = 0.0636, wR ₂ = 0.1503
Largest diff. peak/hole / e Å ⁻³	0.68/-0.23

Table 4. Crystal Data for 1,4-di-*tert*-butyl-1,4,7-triazacyclononane (Figure 3)

Empirical formula	C ₂₈ H ₇₀ Cl ₂ N ₆ O ₃
Formula weight	609.80
Temperature/K	110(2)
Crystal system	monoclinic
Space group	C2/c
a/Å	29.584(3)
b/Å	10.8403(11)
c/Å	23.367(2)
α/°	90
β/°	103.204(2)
γ/°	90
Volume/Å ³	7295.8(13)
Z	8
ρ _{calc} /g/cm ³	1.110
μ/mm ⁻¹	0.212
F(000)	2704.0
Crystal size/mm ³	0.762 × 0.239 × 0.096
Radiation	MoKα (λ = 0.71073)
2θ range for data collection/°	4.014 to 59.762
Index ranges	-41 ≤ h ≤ 40, -15 ≤ k ≤ 15, -32 ≤ l ≤ 32
Reflections collected	46416
Independent reflections	10427 [R _{int} = 0.0413, R _{sigma} = 0.0349]
Data/restraints/parameters	10427/83/477
Goodness-of-fit on F ²	1.014
Final R indexes [I ≥ 2σ (I)]	R ₁ = 0.0471, wR ₂ = 0.1148
Final R indexes [all data]	R ₁ = 0.0623, wR ₂ = 0.1254
Largest diff. peak/hole / e Å ⁻³	0.49/-0.25

Table 5. Crystal Data for 1,2-bis(4,7-di-*tert*-butyl-1,4,7-triazonan-1-yl)ethane (Figure 4)

Empirical formula	C ₃₀ H ₆₄ N ₆
Formula weight	508.87
Temperature/K	110(2)
Crystal system	monoclinic
Space group	C2/c
a/Å	19.0368(19)
b/Å	5.9594(6)
c/Å	28.483(3)
α /°	90
β /°	99.1423(14)
γ /°	90
Volume/Å ³	3190.3(5)
Z	4
ρ_{calc} /cm ³	1.059
μ /mm ⁻¹	0.063
F(000)	1144.0
Crystal size/mm ³	0.993 × 0.164 × 0.118
2 Θ range for data collection/°	4.334 to 58.654
Index ranges	-26 ≤ h ≤ 25, -8 ≤ k ≤ 7, -29 ≤ l ≤ 39
Reflections collected	16949
Independent reflections	4359 [R _{int} = 0.0410, R _{sigma} = 0.0386]
Data/restraints/parameters	4359/13/202
Goodness-of-fit on F ²	1.037
Final R indexes [I ≥ 2 σ (I)]	R ₁ = 0.0547, wR ₂ = 0.1302
Final R indexes [all data]	R ₁ = 0.0731, wR ₂ = 0.1429
Largest diff. peak/hole / e Å ⁻³	0.42/-0.18

Table 6. Crystal Data for Copper (I) 1,2-bis(4,7-di-*tert*-butyl-1,4,7-triazonan-1-yl)ethane (BF₄)₂ (Chart 4a).

Empirical formula	C ₃₄ H ₇₀ B ₂ Cu ₂ F ₈ N ₈
Formula weight	891.68
Temperature/K	110(2)
Crystal system	monoclinic
Space group	P2 ₁ /n
a/Å	10.4244(6)
b/Å	15.4069(9)
c/Å	13.2117(8)
α/°	90
β/°	103.1230(10)
γ/°	90
Volume/Å ³	2066.5(2)
Z	2
ρ _{calc} /g/cm ³	1.433
μ/mm ⁻¹	1.101
F(000)	940
Crystal size/mm ³	0.387×0.218×0.200
2θ range for data collection	4.124 to 62.302
Index ranges	-11 ≤ h ≤ 15, -21 ≤ k ≤ 13, -19 ≤ l ≤ 19
Reflections collected	17302
Independent reflections	6368 [R(int)= 0.0365]
Data/restraints/parameters	6368/67/305
Goodness-of-fit on F ²	1.035
Final R indexes [I>=2σ (I)]	R1=0.0399 wR ₂ =0.0914
Final R indexes [all data]	R1=0.0583, wR ₂ =0.1041
Largest diff. peak/hole/e Å ⁻³	0.61/-0.39

Table 7. Crystal Data for Copper (I) 1,2-bis(4,7-di-*tert*-butyl-1,4,7-triazonan-1-yl)propane (BF₄)₂ (Chart 4b).

Empirical formula	C ₃₅ H ₇₂ B ₂ Cu ₂ F ₈ N ₈
Formula weight	906.47
Temperature/K	110(2)
Crystal system	monoclinic
Space group	P2 ₁ /c
a/Å	14.6422(10)
b/Å	9.1875(6)
c/Å	33.325(2)
α/°	90
β/°	101.9039(10)
γ/°	90
Volume/Å ³	4386.6(5)
Z	4
ρ _{calc} /cm ³	1.373
μ/mm ⁻¹	1.039
F(000)	1913.0
Crystal size/mm ³	0.535 × 0.52 × 0.136
Radiation	MoKα (λ = 0.71073)
2θ range for data collection/°	4.154 to 63.252
Index ranges	-21 ≤ h ≤ 21, -12 ≤ k ≤ 13, -49 ≤ l ≤ 48
Reflections collected	57079
Independent reflections	14542 [R _{int} = 0.0305, R _{sigma} = 0.0295]
Data/restraints/parameters	14542/289/649
Goodness-of-fit on F ²	1.055
Final R indexes [I ≥ 2σ (I)]	R ₁ = 0.0450, wR ₂ = 0.1124
Final R indexes [all data]	R ₁ = 0.0565, wR ₂ = 0.1178
Largest diff. peak/hole / e Å ⁻³	1.16/-0.86

Table 8. Crystal Data for Oxidized Copper 1,2-bis(4,7-di-*tert*-butyl-1,4,7-triazonan-1-yl)ethane (BF₄)₂ (Figure 5).

Empirical formula	C ₃₂ H ₆₇ B _{1.91} Cu ₂ F _{7.62} N ₇ O ₃
Formula weight	890.39
Temperature/K	110(2)
Crystal system	orthorhombic
Space group	Pbca
a/Å	14.4790(8)
b/Å	15.1452(8)
c/Å	38.199(2)
α/°	90
β/°	90
γ/°	90
Volume/Å ³	8376.6(8)
Z	8
ρ _{calc} /cm ³	1.412
μ/mm ⁻¹	1.090
F(000)	3745.0
Crystal size/mm ³	0.48 × 0.354 × 0.204
Radiation	MoKα (λ = 0.71073)
2θ range for data collection/°	3.53 to 56.562
Index ranges	-19 ≤ h ≤ 19, -11 ≤ k ≤ 20, -41 ≤ l ≤ 50
Reflections collected	58984
Independent reflections	10385 [R _{int} = 0.0630, R _{sigma} = 0.0469]
Data/restraints/parameters	10385/357/561
Goodness-of-fit on F ²	1.040
Final R indexes [I ≥ 2σ (I)]	R ₁ = 0.1070, wR ₂ = 0.2782
Final R indexes [all data]	R ₁ = 0.1464, wR ₂ = 0.3047
Largest diff. peak/hole / e Å ⁻³	2.09/-1.37

7.0 References

1. S. Schindler, *Eur. J. Inorg. Chem.* **2000**, 2311-2326.
2. Corder, R.E.; Johnson, E. R., Vega, J. L.; Clausen, E. C.; Gaddy, J. L., *Preprints of Papers - American Chemical Society, Division of Fuel Chemistry*, **1988**, 33(3), 469-78.
3. Hegedus, L.; Soderberg, B. *Transition Metals in the Synthesis of Complex Organic Molecules*; 3rd ed.; University Science Books, **2009**.
4. In *Catalysis without Precious Metals*; Bullock, R. M., Ed.; Wiley-VCH Verlag GmbH & Co. KGaA, **2010**, 277-290.
5. Punniyamurthy, T.; Velusamy, S.; Iqbal, J. *Chem. Rev.* **2005**, 105, 2329-2364.
6. Allen, S. E.; Walvoord, R. R.; Padilla-Salinas, R.; Kozlowski, M. C. *Chem Rev.* **2013**, 113(8), 6234-6458.
7. Karlin, K.D., *Science*. **1993**, 261, 701-708.
8. Lewis, E.A.; W. Tolman, *Chem. Rev.* **2004**, 104(2), 1047-1076.
9. Mahapatra, S.; Halfen, J.A.; Wilkinson, E.C.; Que, L.; Tolman, W.B., *JACS*, **1994**, 116, 9785-9786.
10. Halfen, J.A.; Mahapatra, S.; Wilkinson, E.C.; Kaderli, S.; Young, V.G.; Que, L.; Zuberbühler, A.D.; Tolman, W.B., *Science*, **1996**, 271, 1397-1400
11. Hatcher L.Q.; Karlin, K.D., *J Biol Inorg Chem.* **2004**, 9, 699-683.
12. Decker, H.; Dillinger, R.; Tuczek, F., *Angew Chem Int Ed*, **2000**, 39(9), 1591-95.
13. Himes, R.A.; Barnese, K.; Karlin, K.D., *Angew Chem Int Ed*, **2010**, 49, 6714-6716.
14. Rollff, M.; Schottenheim, J., Decker, H., Tuczek, F., *Chem Soc Rev*, **2011**, 40, 4077-4098.
15. Tolman, W.B., *Accounts of Chemical Research*, **1997**, 30(6), 227-237.
16. Mirica, L. M.; Ottenwaelder, X.; Stack, T. D. P. *Chem Rev*, **2004**, 104(2), 1013-45.
17. Que, L.; Tolman, W.B., *Angew Chem Int Ed*, **2002**, 41, 1114-1137.
18. Itoh, S.; Fukuzumi, S., *Bull Chem Soc Jpn*, **2002**, 75, 2081-2095.
19. Taki, M.; Teramae, S.; Nagatomo, S.; Tachi, Y.; Kitagawa, T.; Itoh, S.; Fukuzumi, S., *JACS*, **2002**, 124, 6367-6377.

-
20. Kunishita, A.; Kubo, M.; Sugimoto, H.; Ogura, T.; Sato, K.; Takui, T.; Itoh, S., *JACS*, **2009**, 131, 2788-89.
 21. Tano, T.; Okubo, Y.; Kunishita, A.; Kubo, M.; Sugimoto, H.; Fujieda, N.; Ogura, T.; Itoh, S., *Inorg Chem*, **2013**, 52, 10431-10437.
 22. Hatcher, L.Q.; Karlin, K.D., *Advances in Inorganic Chemistry*, **2006**, 58, 131-184.
 23. Itoh, S.; Nakao, H.; Berreau, L.M.; Kondo, T.; Komatsu, M.; Fukuzumi, S., *JACS*, 120, 2890-2899.
 24. Lam, B.M.T.; Halfen, J.A.; Young, V.G.; Hagadorn, J.R.; Holland, P.L.; Lledos, A.; Curcurull-Sanchez, L.; Novoa, J.J.; Alvarez, S.; Tolman, W.B., *Inorg Chem*, **2000**, 39, 4059-4072.
 25. Zoppellaro, G.; Sakurai, T.; Huang, H. *J. Biochem.* **2001**, 129, 949-953.
 26. Solomon, E. I.; Chen, P.; Metz, M.; Lee, S.-K.; Palmer, A. E. *Angew. Chem. Int. Ed.* **2001**, 40, 4570-4590.
 27. Kitajima, N.; Yoshihiko, M., *Chem Rev* **1994**, 94, 737-757.
 28. Jacobson, R.R.; Tyeklar, Z.; Farooq, A.; Karlin, K.D.; Liu, S.; Zubieta, J., *JACS*, **1988**, 110, 3690-3692.
 29. Kitajima, N.; Fujisawa, K.; Fujimoto, C.; Moro-oka, Y.; Hashimoto, S.; Kitagawa, T.; Toriumi, K.; Tatsumi, K.; Nakamura, A., *JACS*, **1992**, 114, 1277-1291.
 30. Cruse, R. W.; Kaderli, S.; Karlin, K. D.; Zuberbühler, A. D *JACS*. **1988**, 110, 6882.
 31. Mahapatra, S.; Kaderli, S.; Llobet, A.; Neuhold, Y.; Planche, T.; Halfen, J.A.; Young, V.G.; Kaden, T.A.; Que, L.; Zuberbühler, A.D., Tolman, W.B., *Inorg Chem*, **1997**, 36, 6343-6356.
 32. Blackburn, N.J.; Karlin, K.D.; Concannon, M.; Hayes, J.C.; Gultneh, Y.; Zubieta, J., *Chem Comm*, **1984**, 939-940.
 33. Mahapatra, S.; Halfen, J.A.; Tolman, W.B., *JACS*, **1996**, 118, 11575-11586.
 34. Halfen, J.A.; Young, V.G.; Tolman, W.B., *Inorg Chem*, **1998**, 37, 2102-2103.
 35. Himes, R.A.; Karlin, K.D., *Current Opinion in Chem Biol*, **2009**, 13, 119-131.
 36. Chaudhuri, P.; Wieghardt, K. *Progress in Inorg Chem*, **1987**, 35, 329-436.
 37. Wieghardt, K.; Tolksdorf, I.; Herrmann, W. *Inorg Chem*. **1985**. 24(8), 1230-5.
 38. Krakowiak, K.E.; Bradshaw, J.S.; Izatt, R.M., *J Org. Chem.*, **1990**, 55(10), 3364-68.

-
39. Grenz, A.; Ceccarelli, S.; Bolm, C. *Chem. Commun.* 2001, 1726.
40. Wuts, P. G. M.; Greene, T. W. "Protection for the Amino Group". In *Green's Protective Groups in Organic Synthesis*. John Wiley & Sons, Inc., 2007, 4 ed., 277–290.
41. Theodorou, V.; Ragoussis, V.; Strongilos, A.; Zelepos, E.; Eleftheriou, A.; Dimitriou, M. *Tet Lett.* 2005, 46(8), 1357-1360.
42. Singh, S. B. *Tet Lett.*, 1995, 36, 2009-13.
43. Kindermann, N.; Bill, E.; Dechert, S.; Demeshko, S.; Reijerse, E.J.; Meyer, F., *Angew. Chem. Int. Ed.* 2015, 54, 1738-1743.
44. Blackburn, N.J.; Karlin, K.D.; Concannon, M.; Hayes, J.C.; Gultneh, Y.; Zubieta, J., *Chem Comm*, 1984, 939-940.
45. Hirel, C.; Vostrikova, K. E.; Pecaut, J.; Ovcharenko, V. I.; Rey, P. *Chem Eur J.*, 2001, 7(9), 2007-2014.
46. Thangavel, A.; Wieliczko, M.; Bacsa, J.; Scarborough, C.C. *Inorg Chem.* 2013. 52, 13282-13287.